universität innsbruck

innsbruck Drive and Energy Systems Laboratory

KIT Karlsruher Institut für Technologie

ETI Elektrotechnisches Institut

ETH zürich

Power Electronic Systems Laboratory

Self-Bearing Linear-Rotary Actuators for Future High-Precision Applications

- Kolloquim @KIT\ETI -

Ass. Prof. DDr. Spasoje Mirić

University of Innsbruck, Institute for Mechatronics
Innsbruck Drives and Energy Systems Laboratory (iDES)
www.uibk.ac.at/mechatronik/ides/

October 23, 2023, Online

Outline

- *Introduction*

- *LiRA Examples / Applications*
- *Linear Actuator with Integrated MBs*
- *Position Sensors*
- *Dynamic Modeling, Controller Design*
- *Generalized Complex Space Vector*
- *Double Stator LiRA*

- *Outlook*

universität innsbruck

Introduction

Linear Rotary Actuators (LiRAs)
Applications
LiRA Examples

innsbruck Drive and Energy Systems Laboratory

Linear-Rotary Actuator (LiRA)

- LiRA is conceived by coupling Linear and Rotary actuators (machines)
- Types of coupling: Mechanical, Magnetic, Double Stator

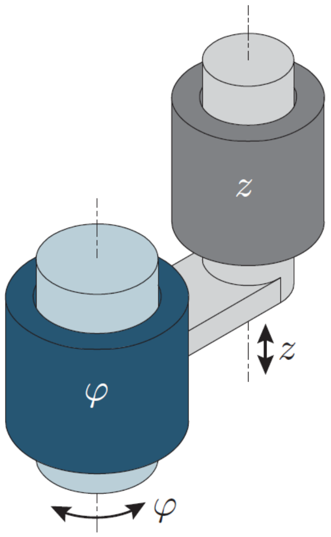

- Parallel Mechanical Coupling

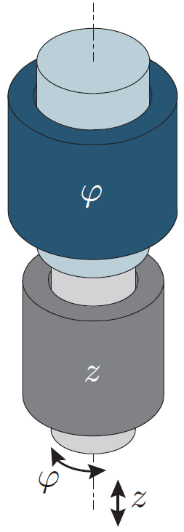

- Series Mechanical Coupling

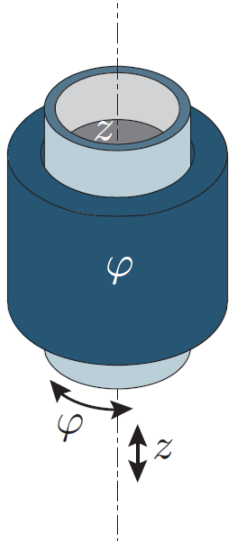

- Double Stator

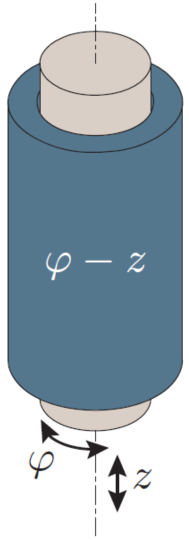

- Magnetic Coupling

- Intended use determines the type of the LiRA, i.e., the type of coupling
- Parallel mechanical coupling → simple to realize, but low dynamics & moving cables

LiRA Application Examples

- A wide spectrum of application areas: servo, tools, industrial automation, robot end-effector, blood pumps

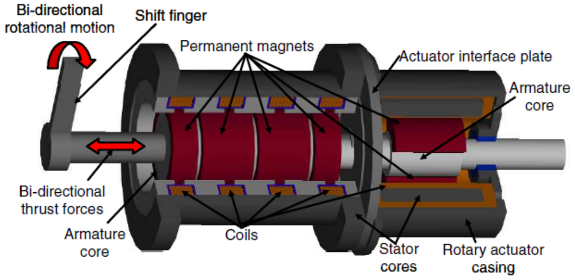

Source: IEEE

- Servo

Source: RIDGID

- Lathe

Source: FOOD manufacture

- Industry Assembly Lines

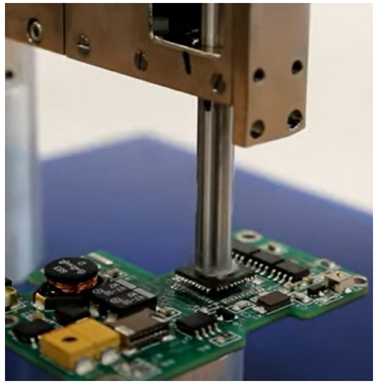

Source: SMAC Moving Coil Actuators

- Pick & Place Robot in Electronics/Semiconductor Industry

Source: camfil

- Handling/Dosing in Pharmaceutical/Chemical Industry

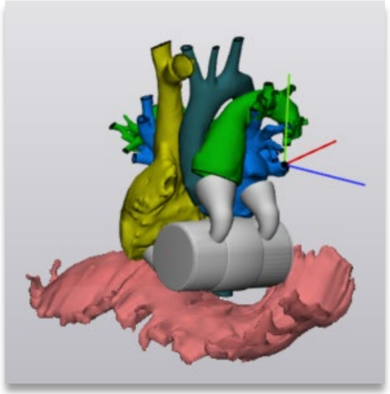

Source: Medizinische Universität Wien

- ShuttlePump

LiRA Example 1

- Series mechanical coupling → three-phase slotless PM rotary actuator (top) & linear actuator (bottom)
- Pick&Place LiRA enables rotational and translational motion for small component placement

Source: IEEE Advancing Technology for Humanity
TU/e EINDHOVEN UNIVERSITY OF TECHNOLOGY

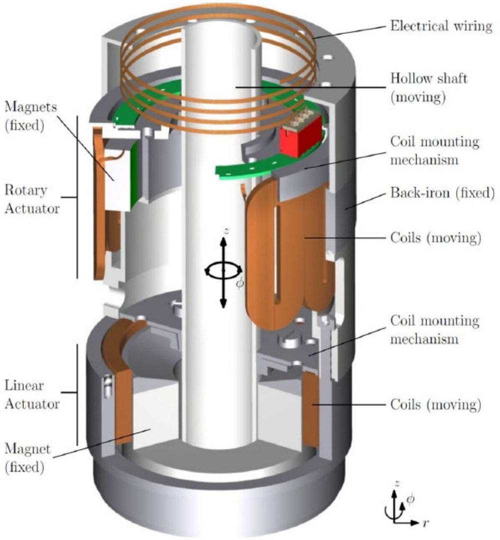

■ LiRA or $z\phi$-Actuator

Parameter	Value
z_{stroke}	± 5 mm
ϕ_{stroke}	$\pm 180°$ degrees
z_{err}	5 µm
ϕ_{err}	3 mrad
α_z	150 m s^{-2}
α_ϕ	7700 rad s^{-2}
v_{max}	3 m s^{-1}
ω_{max}	135 rad s^{-1}
d_z	0.22
d_ϕ	0.39
$L_{z\phi}$	105 mm
$r_{o,max}$	30 mm
$r_{i,min}$	18 mm

■ Specifications

→ High accelerations required

→ Rather a low max. speed

- Component placement throughput → high dynamics/accelerations
- Actuator operation → low speeds due to limited stroke (acceleration/deceleration)

[ref] Overboom, T. T., et al. "Design and Optimization of a Rotary Actuator for a Two-Degree-of-Freedom $ z\phi $-Module." IEEE Transactions on Industry Applications 46.6 (2010): 2401-2409.

LiRA Example 2

- Series mechanical coupling → three-phase rotary actuator & three-phase linear actuator
- Pick&Place LiRA enables rotational and translational motion for small component placement

Source: IEEE, TU/e Eindhoven University of Technology

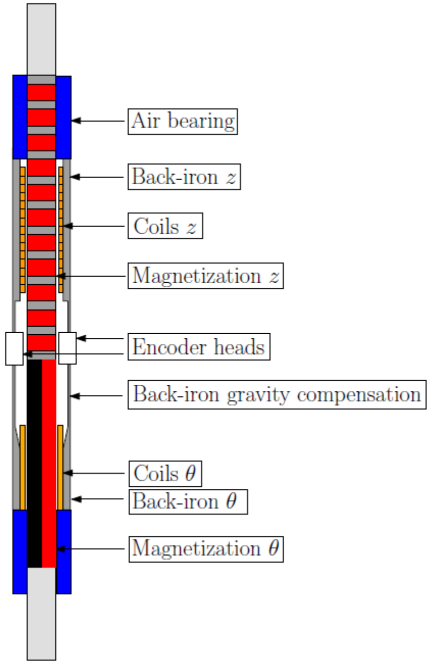

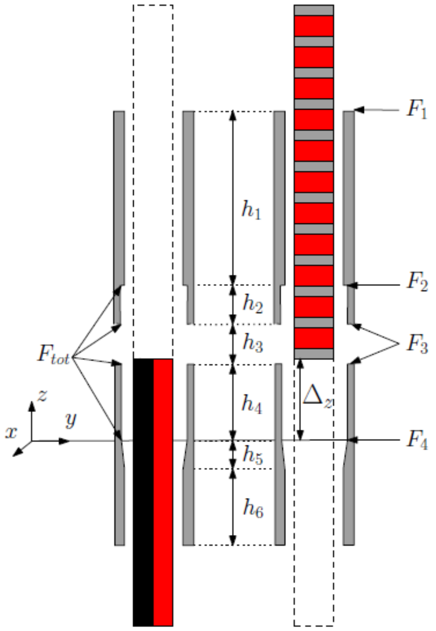

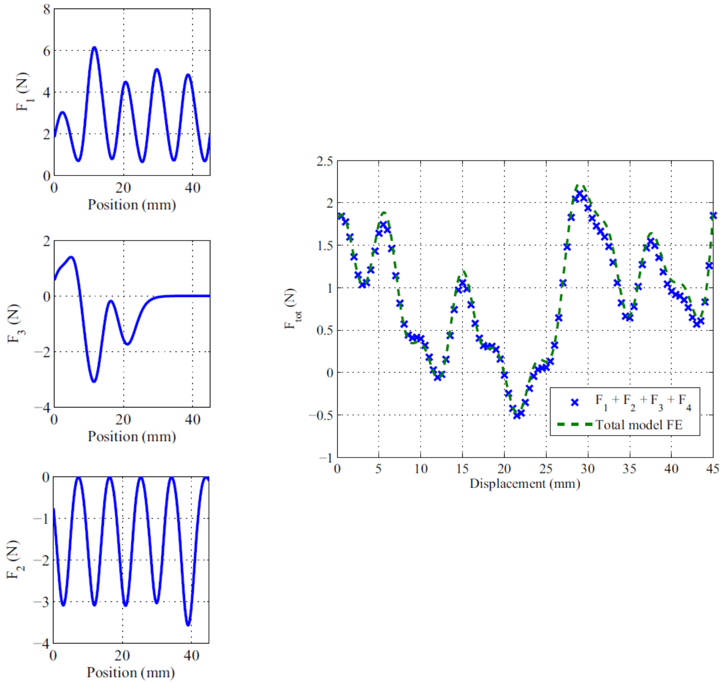

- Cogging force due to end effects → minimization by optimizing stator core geometry / placement
- Passive gravity compensation → force profile optimized in 3D-FEM by varying geometry

[ref] Meessen, K. J., J. J. H. Paulides, and E. A. Lomonova. "Analysis and design considerations of a 2-DoF rotary-linear actuator." 2011 IEEE International Electric Machines & Drives Conference (IEMDC). IEEE, 2011.

LiRA Example 3

- Three-phase rotary actuator & slotless linear actuator winding in the air gap
- Pick&Place LiRA enables rotational and translational motion for small component placement

Source: IEEE Advancing Technology for Humanity

TU/e EINDHOVEN UNIVERSITY OF TECHNOLOGY

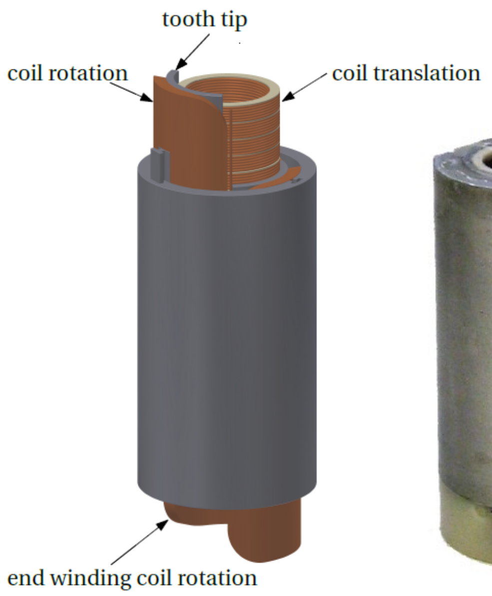

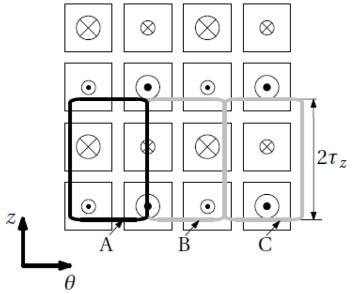

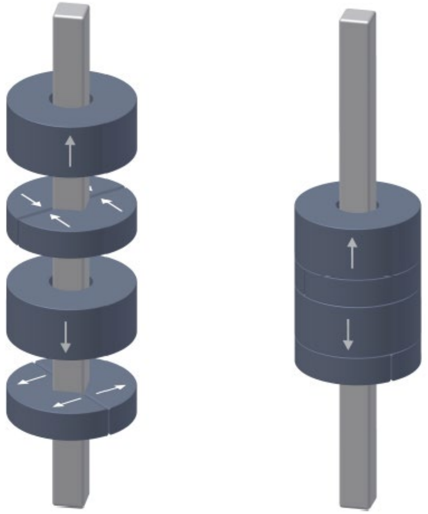

- Single set of mover permanent magnets → special arrangement to interact with rotary and linear windings
- Large air gap → low cogging force; but low machine constant

[ref] Meessen, Koen Joseph. "Electromagnetic fields and interactions in 3D cylindrical structures: Modeling and application." Dept. Electric Eng., Eindhoven Univ. Technol., the Netherlands (2012).

LiRA Example 4

- Moving coil rotary actuator & moving coil linear actuator
- Pick&Place LiRA enables rotational and translational motion for small component placement

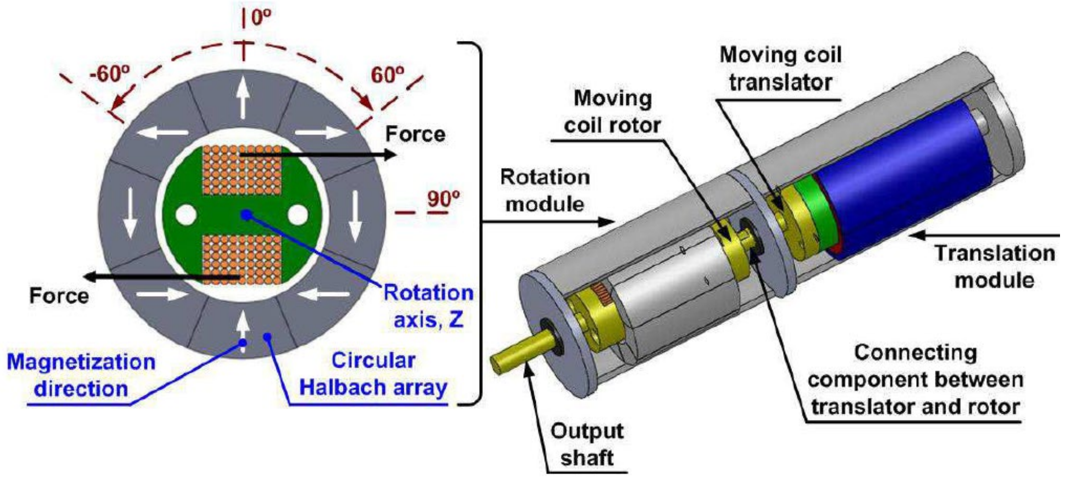

- Limited rotary stroke due to permanent magnet field arrangement → parts with no radial field
- Moving coils → moving cables limit lifetime

[ref] Teo, Tat Joo, et al. "Principle and modeling of a novel moving coil linear-rotary electromagnetic actuator." IEEE Transactions on Industrial Electronics 63.11 (2016): 6930-6940.
https://www.youtube.com/watch?v=ApWlagkbrE0
Agency for Science, Technology and Research, Singapore

LiRA Example 5

- Concentrated coils in linear and rotary direction → 'checkerboard actuator'
- Checkerboard direct drive LiRA enables rotational and translational motion

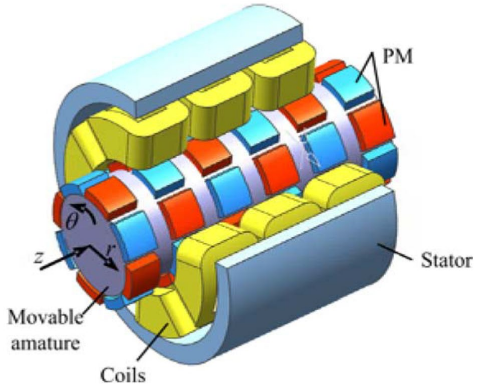

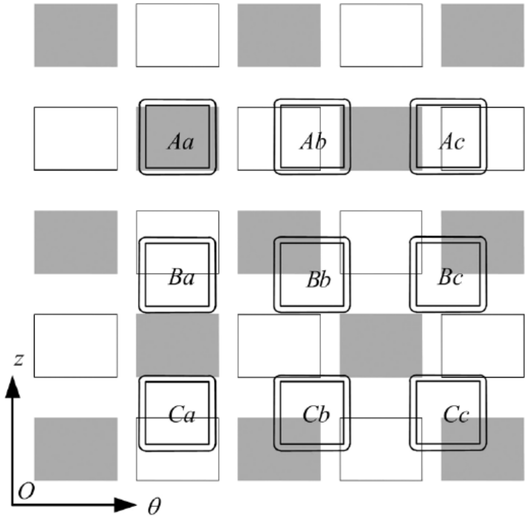

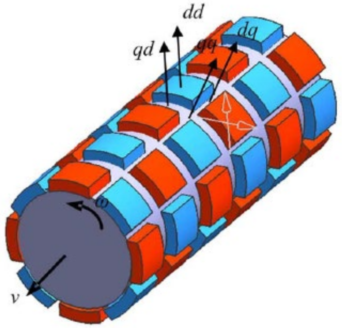

- LiRA with magnetic coupling → highest compactness, increased number of phases, increased control effort
- Ideally no end windings → end winding for the linear direction is an active part of the winding for rotary direction

[ref] Jin, Ping, et al. "3-D analytical linear force and rotary torque analysis of linear and rotary permanent magnet actuator." IEEE transactions on magnetics 49.7 (2013): 3989-3992.

LiRA Example 6

- Double stator LiRA → ‘magnetically insulated’ linear and rotary parts
- Three-phase linear and rotary machines, controlled independently

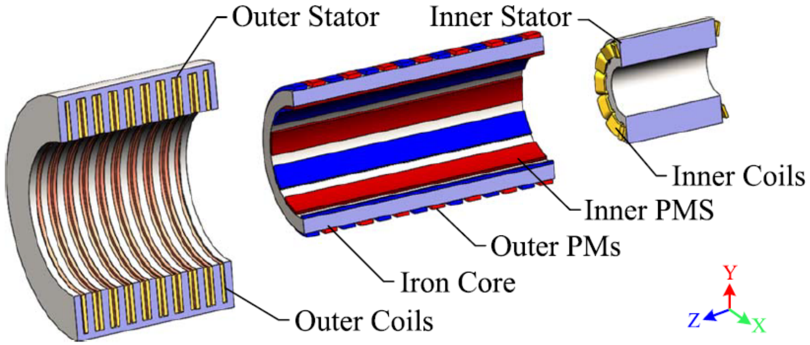

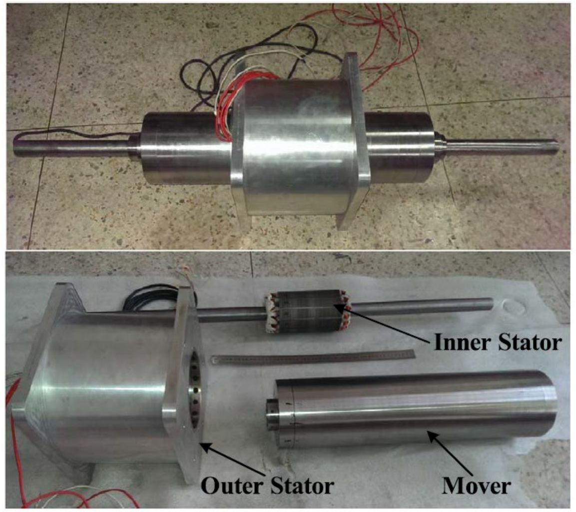

- Large force (650 N) / torque (10 Nm), dynamics limited due to the large moving mass of the mover
- Challenging design → cooling of the inner stator, mover back iron with two sets of PMs

[ref] Xu, Lei, et al. "Design and analysis of a double-stator linear–rotary permanent-magnet motor." IEEE Transactions on Applied Superconductivity 26.4 (2016): 1-4.

LiRA Example 7

- Helical winding (inner and outer) → independent thrust force and torque generation/control
- Slotless LiRA proposed usage for surgery robots in medicine

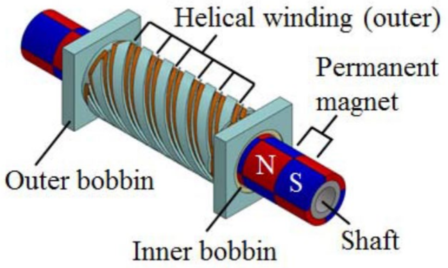

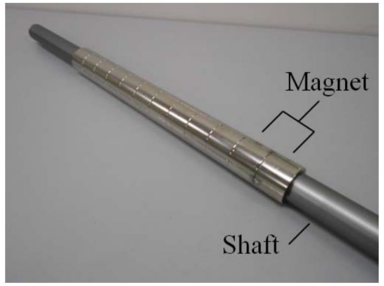

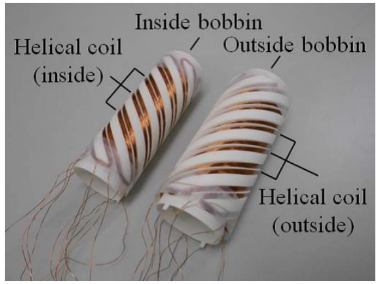

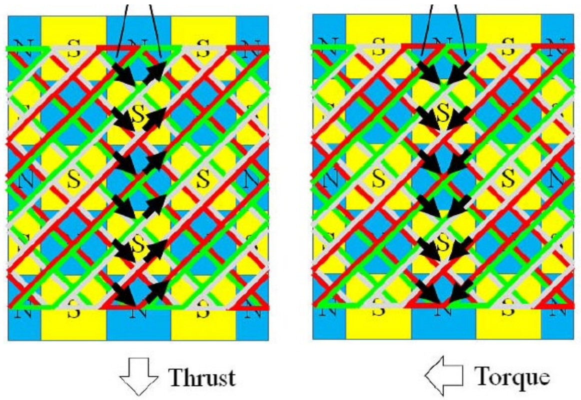

- Limited force (5 N)/torque (0.1 Nm) due to slotless winding, helical winding complicated to realize
- Mover PMs the same as for the checkerboard actuator

[ref] Tanaka, Shodai, Tomoyuki Shimono, and Yasutaka Fujimoto. "Optimal design of length factor for cross-coupled 2-DOF motor with Halbach magnet array." 2015 IEEE International Conference on Mechatronics (ICM). IEEE, 2015.

Need for Improvements

Application Requirements
Conventional Bearings
Bearingless / Self-bearing

High Precision Requirement

- High dynamics robot → reaches accelerations of $150\ ^{\mathrm{m}}/_{\mathrm{s}^2}$ and speeds of $5\ ^{\mathrm{m}}/_{\mathrm{s}}$
- Horizontal workspace of $300\ \mathrm{mm} \times 300\ \mathrm{mm}$; repeatability $< 10\ \mu\mathrm{m}$

Source: euspen

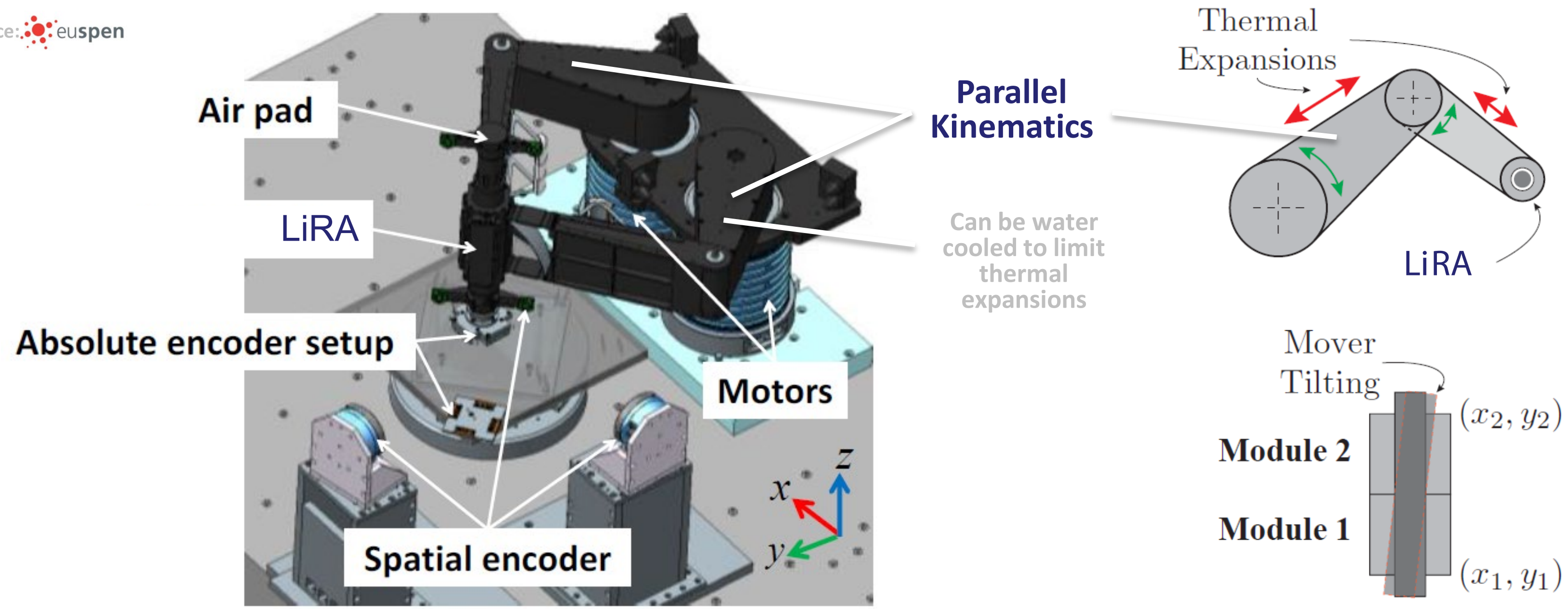

- Thermal expansions in parallel kinematics deteriorate precision → LiRA with radial position control
- Handling smaller components/dies → mover tilting necessary
- Mechanical/air bearings used in conventional LiRAs can not control radial position nor tilting

High Purity Requirement

- Applications requiring high purity → clean rooms, bioprocessing, pharmaceutical
- Mechanical bearings → limited lifetime / limited purity levels / often disassembling for cleaning

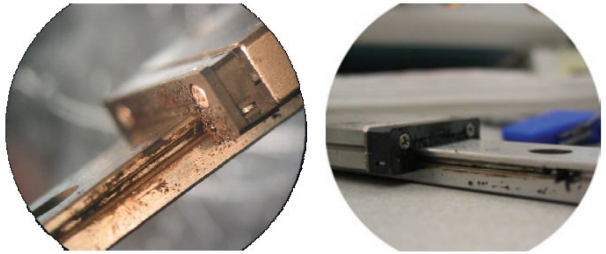

- Mechanical bearings compromise high purity

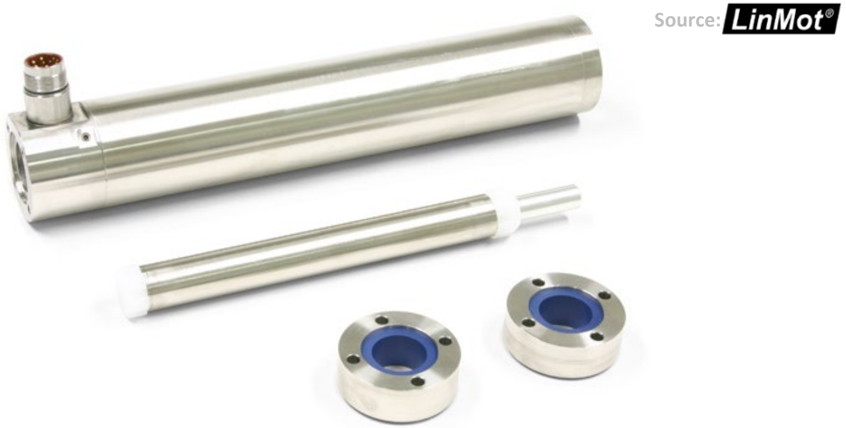

- Disassembling for regular high-pressure washdowns

- Air bearings → require air supply / prohibited operation in low-pressure environments
- High precision & high purity requirements limit usage of LiRAs with conventional bearings

[ref] Paulides, Johannes JH, Jeroen LG Janssen, and Elena A. Lomonova. "Bearing lifetime of linear PM machines." *2009 IEEE Energy Conversion Congress and Exposition*. IEEE, 2009.

Magnetic Bearings (MBs)

- Magnetic bearings → generate radial forces to keep the rotor/mover centered
- Closed loop position controller → sensor, microcontroller, power converter, MB windings

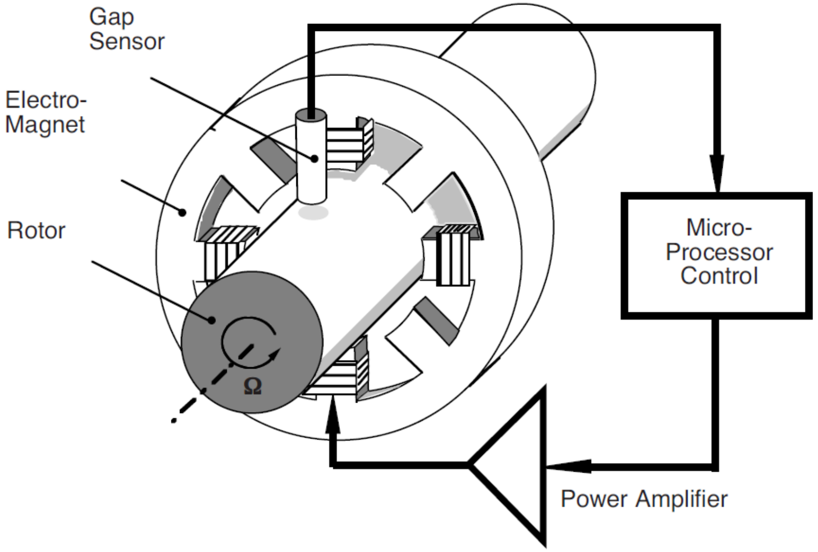

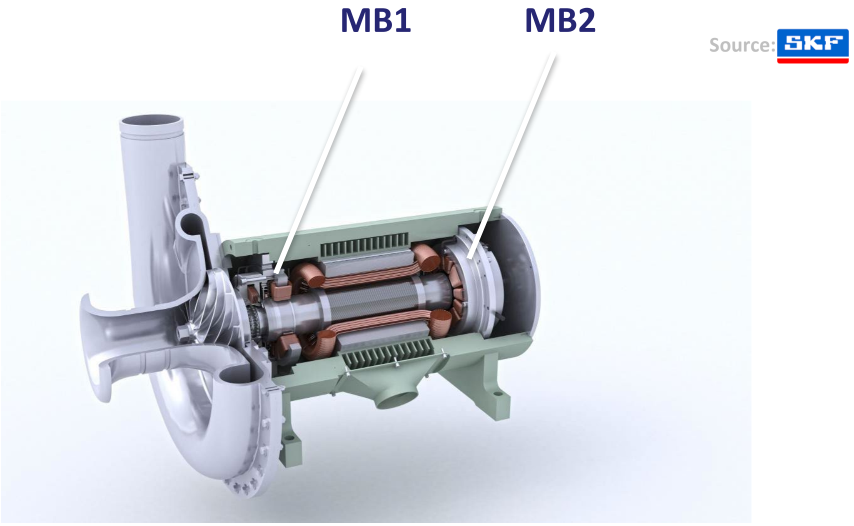

- Characteristics → free of contact, no contaminating wear, bearing stiffness control, low maintenance
- Applications → vacuum and clean room system, high-speed pumps, high-purity pumps, flywheels

[ref] Maslen, Eric H., and Gerhard Schweitzer, eds. Magnetic bearings: theory, design, and application to rotating machinery. Berlin, Heidelberg: Springer-Verlag Berlin Heidelberg, 2009.

Standalone MBs and Self-bearing/Bearingless Machines

- Self-bearing/Bearingless → integrate MBs into the existing machine structure
- Achieve self-bearing function → superimpose the main field (torque, p poles) with the $p \pm 2$ type

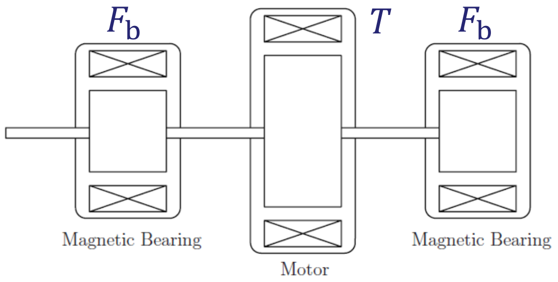

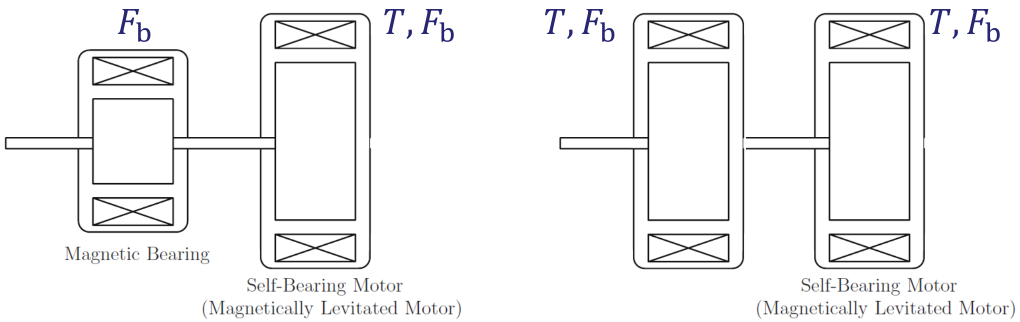

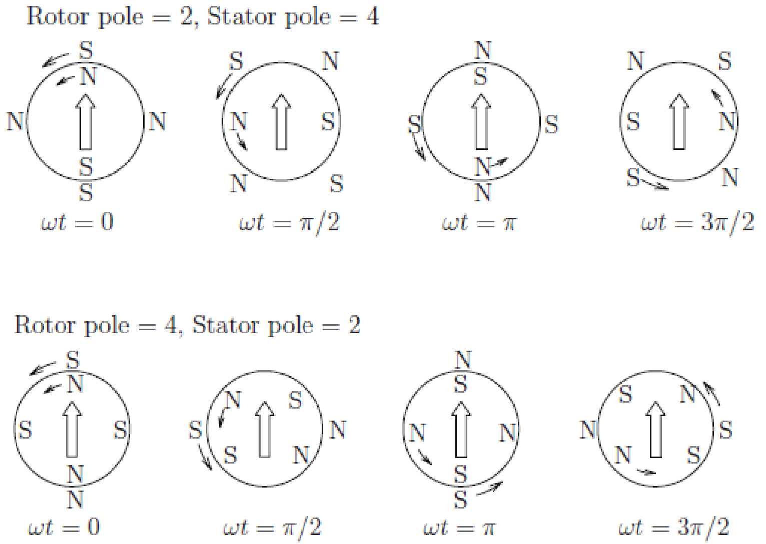

P+2

P-2

- Tilting control of the long shaft → either (F_b) & (T, F_b) or (T, F_b) & (T, F_b)
- $p \pm 2$ type is achieved by winding scheme or current distribution in the existing main windings

[ref] Maslen, Eric H., and Gerhard Schweitzer, eds. Magnetic bearings: theory, design, and application to rotating machinery. Berlin, Heidelberg: Springer-Verlag Berlin Heidelberg, 2009.

The Challenge: LiRA with MBs

- Integrating MBs into a LiRA → various combinations of standalone and self-bearing options are possible
- Tilting control of the mover necessary → MBs always at each axial end of a LiRA

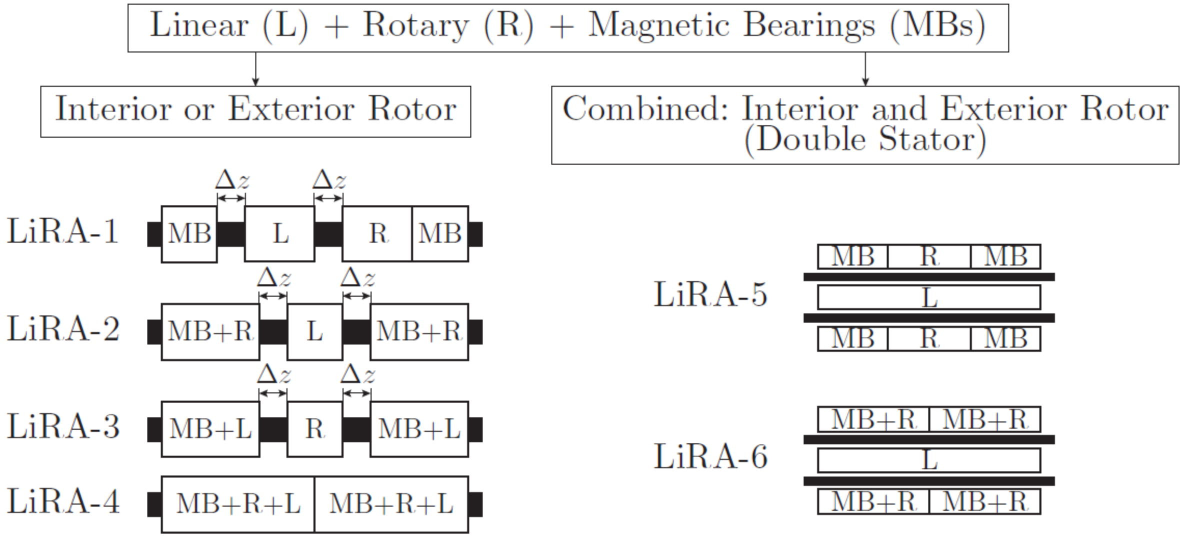

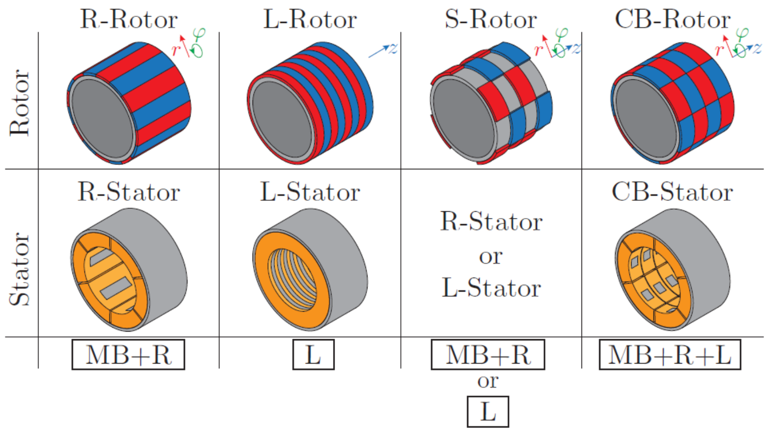

- Distance between the segments Δz = linear stroke → due to different PM arrangements in the mover
- MB + R → conventional; MB + L → interesting for further investigation!

[ref] Mirić, Spasoje, Dominik Bortis, and Johann Walter Kolar. "Design and comparison of permanent magnet self-bearing linear-rotary actuators." 2019 12th International Symposium on Linear Drives for Industry Applications (LDIA). IEEE, 2019.

Linear Actuator with Integrated MBs

Topology Derivation
Bearing Force Generation
Inverter Supply Requirements

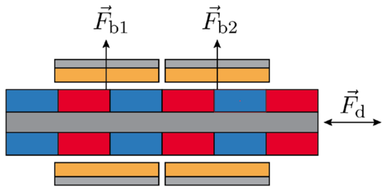

Tubular Linear Actuator Derivation

- Derivation of TLA → tangential force for generating T in RA, generates drive F_d force in TLA
- TLA has fewer stray field compared to FLA due to the closed structure

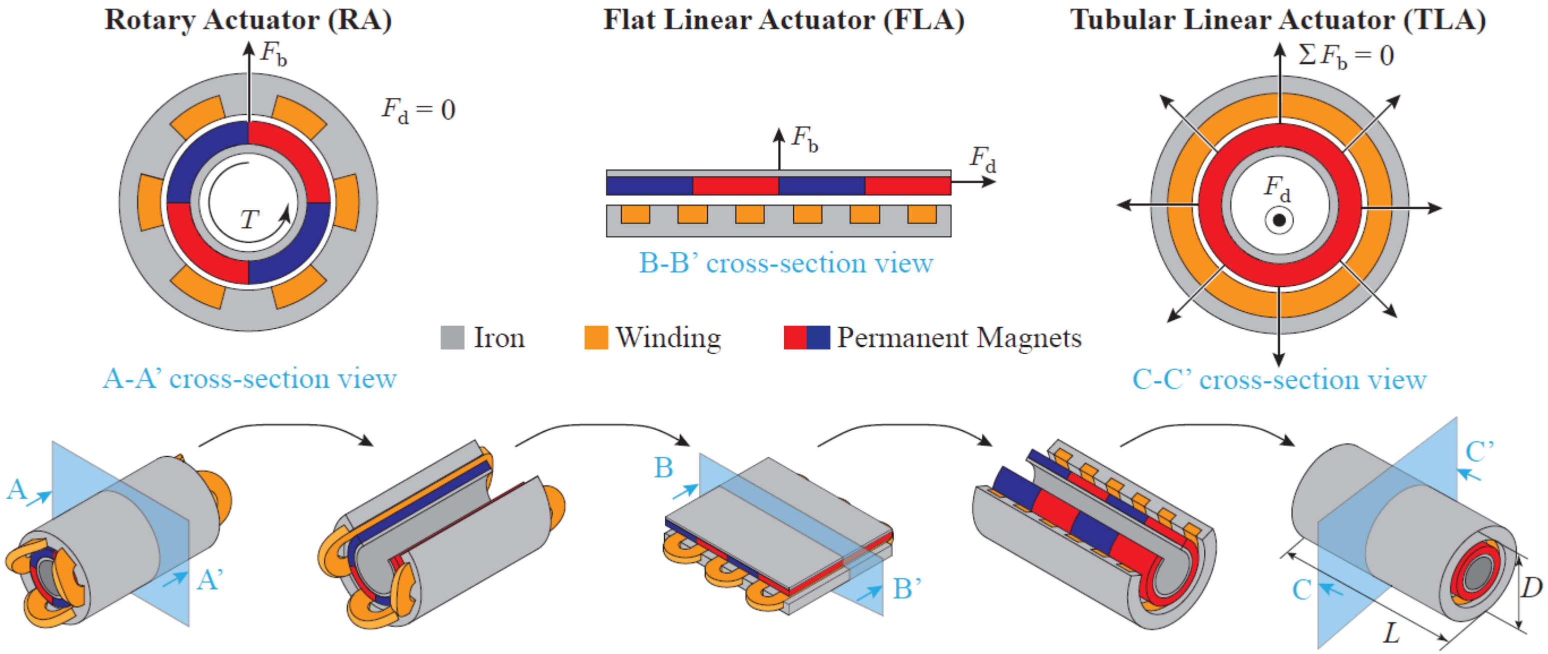

- TLA has circumferential symmetry → it can not generate bearing (radial) force, i.e., no MBs are possible
- FLA can generate bearing force F_b, but there is an attraction force between the mover PMs and the stator iron

[ref] Mirić, Spasoje, Johann W. Kolar, and Dominik Bortis. "Novel tubular linear actuator with integrated magnetic bearing." e & i Elektrotechnik und Informationstechnik 139.2 (2022): 230-242.

Tubular Linear Actuator (TLA)

- Three-phase ring windings → maximum usage of copper, no end winding
- d axis aligned with the peak flux density wave of the mover; θ is the electrical angle in a linear direction

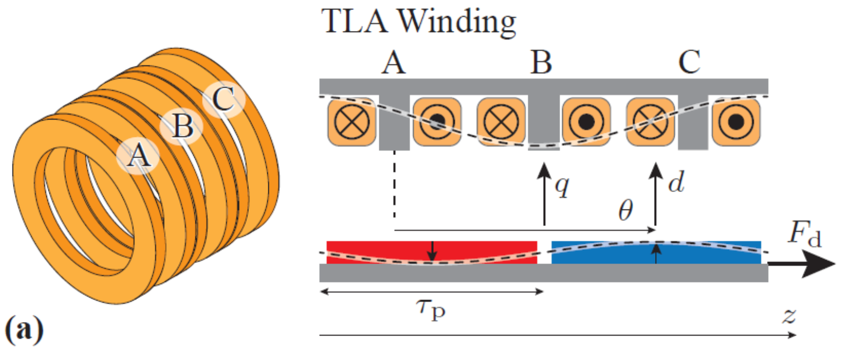

(a)

$$\begin{bmatrix} x_A^d & x_B^d & x_C^d \end{bmatrix} = \begin{bmatrix} x_d & x_q \end{bmatrix} \times \begin{bmatrix} \cos(\theta+\gamma_A) & \cos(\theta+\gamma_B) & \cos(\theta+\gamma_C) \\ -\sin(\theta+\gamma_A) & -\sin(\theta+\gamma_B) & -\sin(\theta+\gamma_C) \end{bmatrix}$$

(b)

Linear Direction

$$\begin{bmatrix} x_d & x_q \end{bmatrix} = \begin{bmatrix} x_A^d & x_B^d & x_C^d \end{bmatrix} \times \frac{2}{3} \begin{bmatrix} \cos(\theta+\gamma_A) & -\sin(\theta+\gamma_A) \\ \cos(\theta+\gamma_B) & -\sin(\theta+\gamma_B) \\ \cos(\theta+\gamma_C) & -\sin(\theta+\gamma_C) \end{bmatrix}$$

Linear Direction

(c)

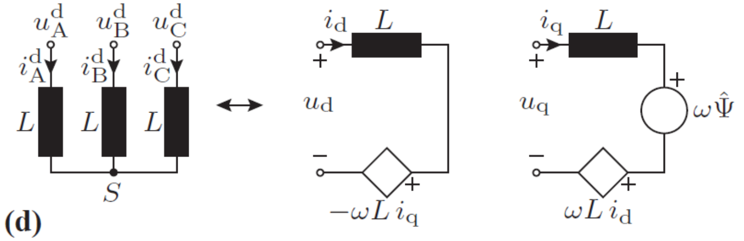

(d)

$$\gamma_A = 0,\ \gamma_B = -2\pi/3,\ \gamma_C = 2\pi/3$$

$$i_A^d = \hat{I}_d \cos(\theta + \theta_i^d + \gamma_A)$$
$$i_B^d = \hat{I}_d \cos(\theta + \theta_i^d + \gamma_B)$$
$$i_C^d = \hat{I}_d \cos(\theta + \theta_i^d + \gamma_C)$$

$$i_d^* = 0 \qquad i_q^* = \hat{I}_d = \frac{F_d^*}{K_d} \qquad K_d = \frac{3\pi}{2\tau_p}\hat{\Psi}$$

- TLA can generate linear drive force F_d; bearing force F_b is not possible to achieve with the TLA
- dq coordinated in a linear direction → stationary coordinates representation of the three-phase winding

[ref] Mirić, Spasoje, Dominik Bortis, and Johann Walter Kolar. "Design and comparison of permanent magnet self-bearing linear-rotary actuators." 2019 12th International Symposium on Linear Drives for Industry Applications (LDIA). IEEE, 2019.

xy Winding for Bearing Force Generation/Control

- A coil of the TLA split into 4 pieces, $x-$ and $y-$direction → bearing force F_{b} generation possible
- Bearing force generation capability → depends on the linear position of the mover/PM poles

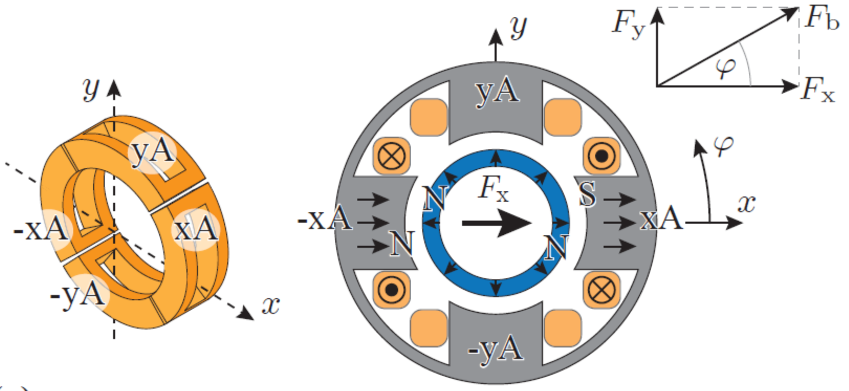

(a)

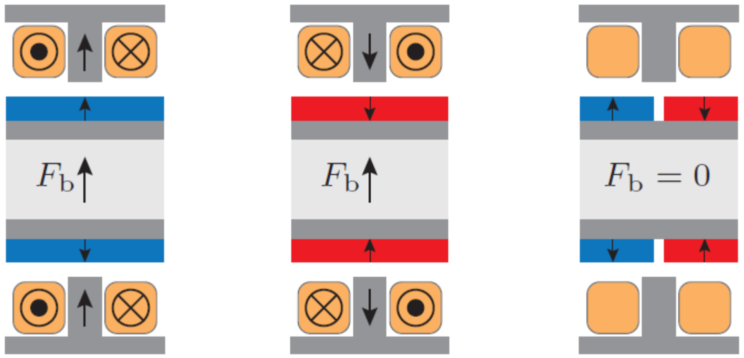

(c.i) (c.ii) (c.iii)

$$F_{\mathrm{b}} = \sqrt{F_{\mathrm{x}}^2 + F_{\mathrm{x}}^2}$$

$$\varphi = \arctan 2(F_{\mathrm{x}}, F_{\mathrm{y}})$$

$$i_{\mathrm{x}}^* = \frac{F_{\mathrm{x}}^*}{K_{\mathrm{b}}} = \hat{I}_{\mathrm{b}} \cos(\varphi)$$

$$i_{\mathrm{y}}^* = \frac{F_{\mathrm{y}}^*}{K_{\mathrm{b}}} = \hat{I}_{\mathrm{b}} \sin(\varphi)$$

- $d-$ current component in a linear direction needed!

- F_{b} generation possible if PM is facing the stator teeth → as long as there is non-zero flux linkage
- Mover/PM linear position changes in during the operation of the actuator

[ref] Mirić, Spasoje, Dominik Bortis, and Johann Walter Kolar. "Design and comparison of permanent magnet self-bearing linear-rotary actuators." 2019 12th International Symposium on Linear Drives for Industry Applications (LDIA). IEEE, 2019.

xy Winding and Three-Phase ABC Linear Winding

- Bearing force currents → 'd – component' in a linear direction, must not generate drive (linear) force
- xy – current components (circumferential) → determined by the desired force direction

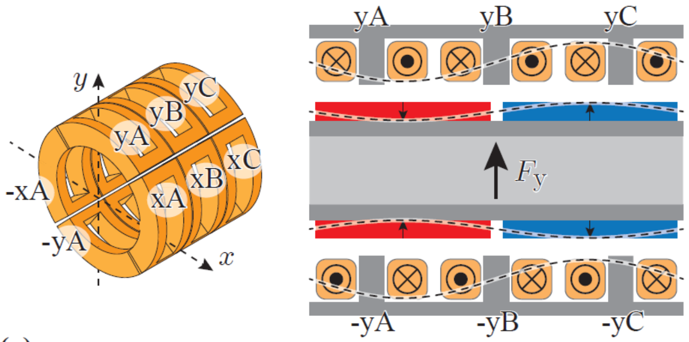

(a)

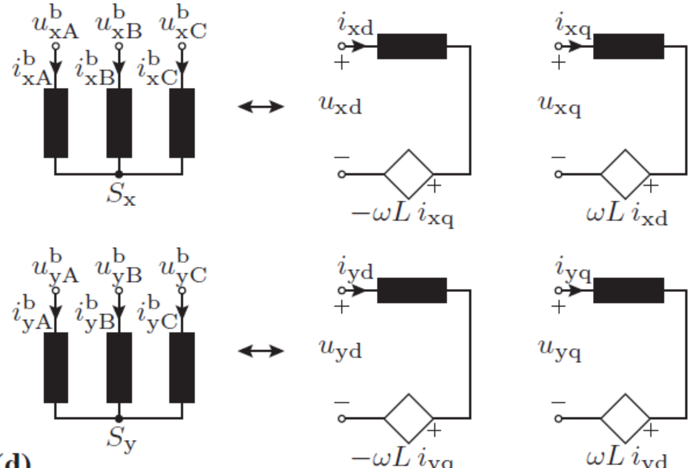

(d)

$$i^*_{xd} = i^*_x = \frac{F^*_x}{K_b} \qquad i^*_{xq} = 0$$

$$i^*_{yd} = i^*_y = \frac{F^*_y}{K_b} \qquad i^*_{yq} = 0,$$

$$i^*_{x\{A,B,C\}} = i^*_{xd} \cdot \cos(\theta + \theta^b_i + \gamma_{\{A,B,C\}})$$
$$i^*_{y\{A,B,C\}} = i^*_{yd} \cdot \cos(\theta + \theta^b_i + \gamma_{\{A,B,C\}})$$

- i^*_{xd} and i^*_{yd} calculated from the force components that should act on the mover (e.g., obtained by position controller)
- θ is the electrical angle determined by the mover's axial position z → $\theta = \pi \cdot z/\tau_p$

[ref] Mirić, Spasoje, Dominik Bortis, and Johann Walter Kolar. "Design and comparison of permanent magnet self-bearing linear-rotary actuators." 2019 12th International Symposium on Linear Drives for Industry Applications (LDIA). IEEE, 2019.

$xydq$ Transformation

- 4 stationary components → xy for bearing force (rotary dir.) & dq for drive force (linear dir.)
- Variable x can be votage v, current i or flux linkage ψ

Linear Direction

Rotary Direction

$$\underbrace{\begin{bmatrix} x_{\mathrm{xd}} & x_{\mathrm{xq}} \\ x_{\mathrm{yd}} & x_{\mathrm{yq}} \end{bmatrix}}_{\mathrm{xydq}} = \underbrace{\begin{bmatrix} x^{\mathrm{b}}_{\mathrm{xA}} & x^{\mathrm{b}}_{\mathrm{xB}} & x^{\mathrm{b}}_{\mathrm{xC}} \\ x^{\mathrm{b}}_{\mathrm{yA}} & x^{\mathrm{b}}_{\mathrm{yB}} & x^{\mathrm{b}}_{\mathrm{yC}} \end{bmatrix}}_{\mathrm{xyABC}} \times \frac{2}{3} \begin{bmatrix} \cos(\theta + \gamma_{\mathrm{A}}) & -\sin(\theta + \gamma_{\mathrm{A}}) \\ \cos(\theta + \gamma_{\mathrm{B}}) & -\sin(\theta + \gamma_{\mathrm{B}}) \\ \cos(\theta + \gamma_{\mathrm{C}}) & -\sin(\theta + \gamma_{\mathrm{C}}) \end{bmatrix}$$

Linear Direction

$xydq$ Transformation

Linear Direction

Rotary Direction

$$\underbrace{\begin{bmatrix} x^{\mathrm{b}}_{\mathrm{xA}} & x^{\mathrm{b}}_{\mathrm{xB}} & x^{\mathrm{b}}_{\mathrm{xC}} \\ x^{\mathrm{b}}_{\mathrm{yA}} & x^{\mathrm{b}}_{\mathrm{yB}} & x^{\mathrm{b}}_{\mathrm{yC}} \end{bmatrix}}_{\mathrm{xyABC}} = \underbrace{\begin{bmatrix} x_{\mathrm{xd}} & x_{\mathrm{xq}} \\ x_{\mathrm{yd}} & x_{\mathrm{yq}} \end{bmatrix}}_{\mathrm{xydq}} \times \begin{bmatrix} \cos(\theta + \gamma_{\mathrm{A}}) & \cos(\theta + \gamma_{\mathrm{B}}) & \cos(\theta + \gamma_{\mathrm{C}}) \\ -\sin(\theta + \gamma_{\mathrm{A}}) & -\sin(\theta + \gamma_{\mathrm{B}}) & -\sin(\theta + \gamma_{\mathrm{C}}) \end{bmatrix}$$

Inverse $xydq$ Transformation

- 12 phase windings, but 6 phase quantities → windings on the same axis connected in series
- Linear direction → ABC – three-phase quantities; dq – stationary coordinates quantities

[ref] Mirić, Spasoje, Dominik Bortis, and Johann Walter Kolar. "Design and comparison of permanent magnet self-bearing linear-rotary actuators." 2019 12th International Symposium on Linear Drives for Industry Applications (LDIA). IEEE, 2019.

abc Winding for Bearing and ABC Winding for Linear Motion

- Bearing force control with a three-phase winding abc → xy current components determine the $\hat{I}_\mathrm{b}$ and φ
- φ - electrical angle for rotary direction; θ – electrical angle for linear direction

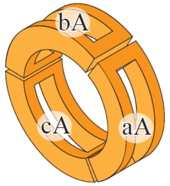

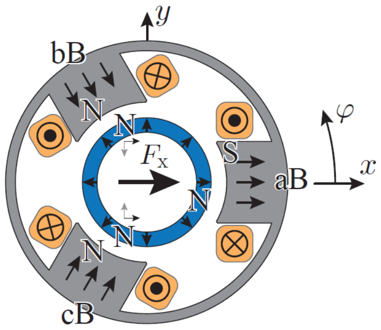

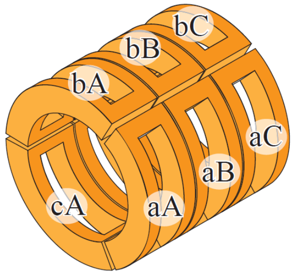

$$i^*_\mathrm{xd} = i^*_\mathrm{x} = \frac{F^*_\mathrm{x}}{K_\mathrm{b}} \qquad i^*_\mathrm{xq} = 0$$

$$i^*_\mathrm{yd} = i^*_\mathrm{y} = \frac{F^*_\mathrm{y}}{K_\mathrm{b}} \qquad i^*_\mathrm{yq} = 0,$$

$$\hat{I}_\mathrm{b} = \sqrt{(i^*_\mathrm{xd})^2 + (i^*_\mathrm{yd})^2}$$

$$\varphi = \arctan 2(i^*_\mathrm{xd}, i^*_\mathrm{yd})$$

$$i^\mathrm{b}_{\mathrm{a}\{\mathrm{A,B,C}\}} = \hat{I}_\mathrm{b}\cos(\varphi + \gamma_\mathrm{a}) \cdot \cos(\theta + \theta^\mathrm{b}_\mathrm{i} + \gamma_{\{\mathrm{A,B,C}\}})$$

$$i^\mathrm{b}_{\mathrm{b}\{\mathrm{A,B,C}\}} = \hat{I}_\mathrm{b}\cos(\varphi + \gamma_\mathrm{b}) \cdot \cos(\theta + \theta^\mathrm{b}_\mathrm{i} + \gamma_{\{\mathrm{A,B,C}\}})$$

$$i^\mathrm{b}_{\mathrm{c}\{\mathrm{A,B,C}\}} = \hat{I}_\mathrm{b}\cos(\varphi + \gamma_\mathrm{c}) \cdot \cos(\theta + \theta^\mathrm{b}_\mathrm{i} + \gamma_{\{\mathrm{A,B,C}\}})$$

$$\gamma_\mathrm{A} = 0,\ \gamma_\mathrm{B} = -2\pi/3,\ \gamma_\mathrm{C} = 2\pi/3$$

- Comparison between xy and abc winding type → capability for the bearing F_b and the drive F_d force generation
- Rotary direction → abc – three-phase quantities; xy – stationary coordinates quantities

[ref] Mirić, Spasoje, Dominik Bortis, and Johann Walter Kolar. "Design and comparison of permanent magnet self-bearing linear-rotary actuators." 2019 12th International Symposium on Linear Drives for Industry Applications (LDIA). IEEE, 2019.

abcdq Transformation

- 4 stationary components → xy for bearing force (rotary dir.) & dq for drive force (linear dir.)
- Variable x can be votage v, current i or flux linkage ψ

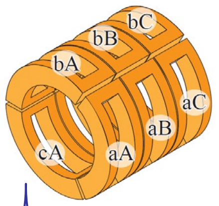

Rotary Direction

$$\underbrace{\begin{bmatrix} x_{\mathrm{xd}} & x_{\mathrm{xq}} \\ x_{\mathrm{yd}} & x_{\mathrm{yq}} \end{bmatrix}}_{\mathrm{xydq}} = \underbrace{\frac{2}{3}\begin{bmatrix} \cos(\gamma_{\mathrm{a}}) & \cos(\gamma_{\mathrm{b}}) & \cos(\gamma_{\mathrm{c}}) \\ -\sin(\gamma_{\mathrm{a}}) & -\sin(\gamma_{\mathrm{b}}) & -\sin(\gamma_{\mathrm{c}}) \end{bmatrix}}_{\mathrm{abc} \rightarrow \mathrm{xy}} \times \underbrace{\begin{bmatrix} x^{\mathrm{b}}_{\mathrm{aA}} & x^{\mathrm{b}}_{\mathrm{aB}} & x^{\mathrm{b}}_{\mathrm{aC}} \\ x^{\mathrm{b}}_{\mathrm{bA}} & x^{\mathrm{b}}_{\mathrm{bB}} & x^{\mathrm{b}}_{\mathrm{bC}} \\ x^{\mathrm{b}}_{\mathrm{cA}} & x^{\mathrm{b}}_{\mathrm{cB}} & x^{\mathrm{b}}_{\mathrm{cC}} \end{bmatrix}}_{\mathrm{abcABC}} \times \underbrace{\frac{2}{3}\begin{bmatrix} \cos(\theta+\gamma_{\mathrm{A}}) & -\sin(\theta+\gamma_{\mathrm{A}}) \\ \cos(\theta+\gamma_{\mathrm{B}}) & -\sin(\theta+\gamma_{\mathrm{B}}) \\ \cos(\theta+\gamma_{\mathrm{C}}) & -\sin(\theta+\gamma_{\mathrm{C}}) \end{bmatrix}}_{\mathrm{ABC} \rightarrow \mathrm{dq}}$$

abcdq Transformation

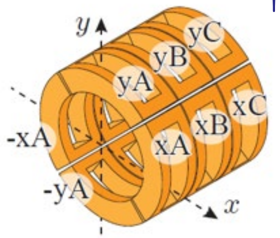

- *abcABC* winding, three-phase rotary and three-phase linear → 9 phase quantities
- Bearing current component & Drive current component → *combined* or *separated* windings

[ref] Mirić, Spasoje, Dominik Bortis, and Johann Walter Kolar. "Design and comparison of permanent magnet self-bearing linear-rotary actuators." 2019 12th International Symposium on Linear Drives for Industry Applications (LDIA). IEEE, 2019.

$xyABC$ Winding Inverter Supply

- Bearing force and driving force function → realized with the *combined* or *separated* windings
- Combined winding → each phase winding contains the *bearing* and the *drive* current components

Combined winding, 12 half-bridges

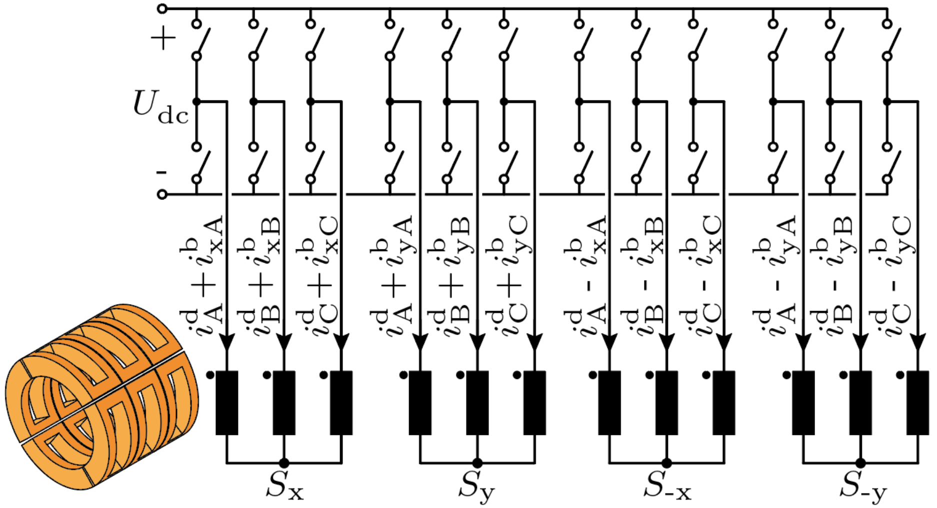

Separated winding, 9 half-bridges

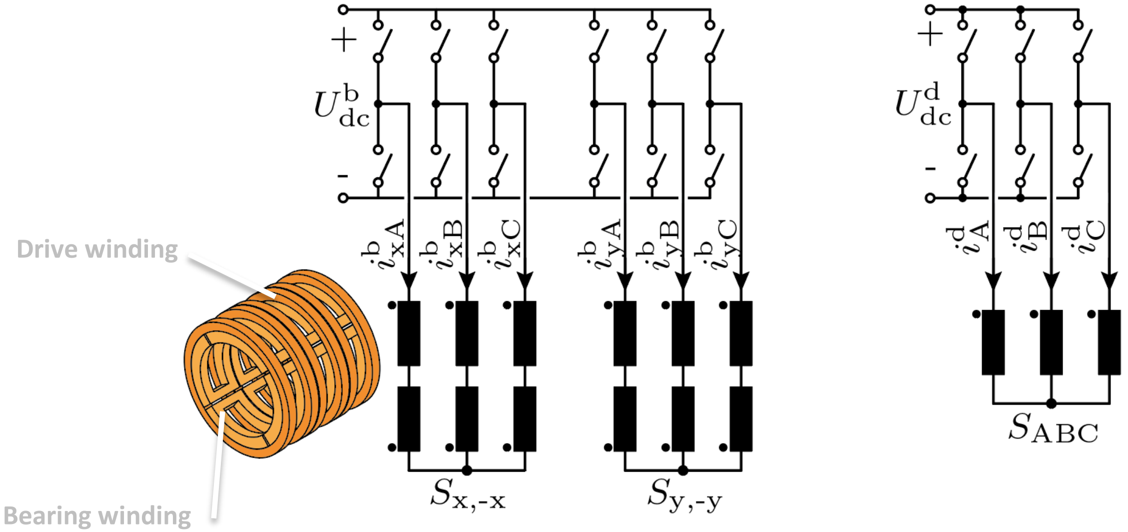

- Combined winding → each winding needs a dedicated half-bridge; star points with the linear three-phase system
- Separated winding → anti-series connection of the bearing windings, no induced back EMF

[ref] Mirić, Spasoje, Dominik Bortis, and Johann Walter Kolar. "Design and comparison of permanent magnet self-bearing linear-rotary actuators." 2019 12th International Symposium on Linear Drives for Industry Applications (LDIA). IEEE, 2019.

abcABC Winding Inverter Supply

- Bearing force and driving force function → realized with the *combined* or *separated* windings
- Combined winding → each phase winding contains the *bearing* and the *drive* current components

Combined winding, 9 half-bridges

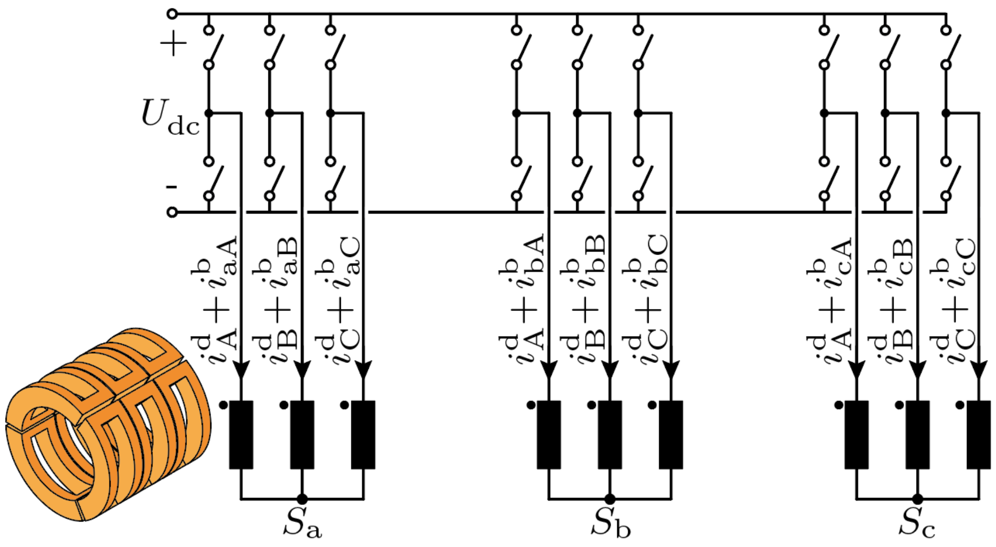

Separated winding, 12 half-bridges

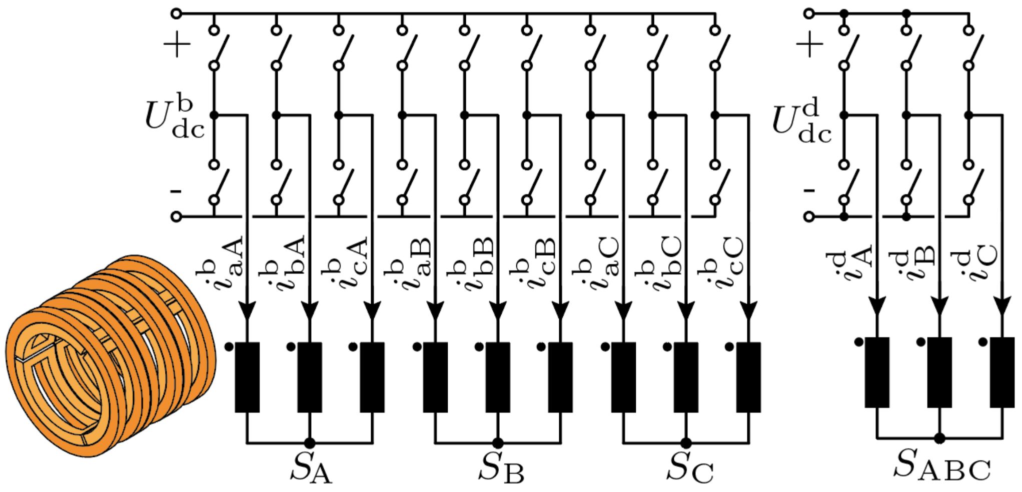

- Combined winding → each winding needs a dedicated half-bridge; star points with the linear three-phase system
- Comparison in terms of the bearing and the drive force generation capability → combined versus separated windings

[ref] Mirić, Spasoje, Dominik Bortis, and Johann Walter Kolar. "Design and comparison of permanent magnet self-bearing linear-rotary actuators." 2019 12th International Symposium on Linear Drives for Industry Applications (LDIA). IEEE, 2019.

Comparison of the Winding Types

- Magnetically Levitated Tubular Actuator (MALTA)
- 2 modules necessary to control the tilting of the mover

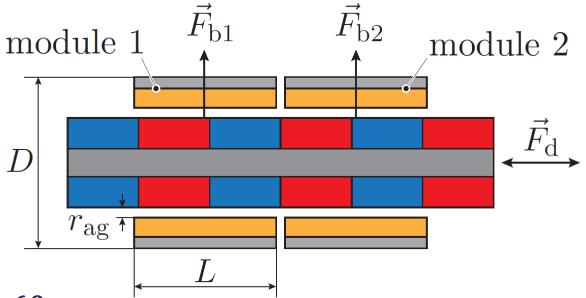

$L = 60$ mm
$D = 60$ mm
$r_{ag} = 2$ mm

- MALTA

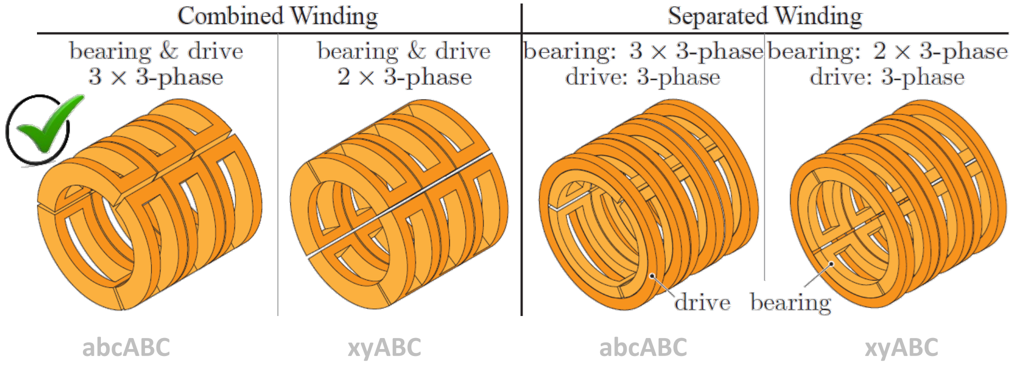

Winding Realization	Shown	Force/$F_{d,TLA}$ Drive	Bearing	Number of Half-bridges
Combined				
3 × 3-phase	Fig. 4.10(a)	0.78	1.12	18
2 × 3-phase	Fig. 4.10(b)	0.76	1.1	24
Separated				
3 × 3-phase +3-phase	Fig. 4.10(c)	0.57	0.81	24
2 × 3-phase +3-phase	Fig. 4.10(d)	0.29	0.46	18

→ for 2 modules

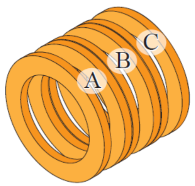

TLA Winding: benchmark for comparison

- Comparison with respect to the driving force of the conventional TLA; 15 W of copper losses; fixed volume
- $abcABC$ winding or 3 × 3 phase MALTA → the largest forces; the lowest number of the inverter half-bridges

[ref] Spasoje Miric, 'Linear-Rotary Bearingless Actuators,', PhD Thesis, ETH Zurich, 2021.

MALTA Prototype Design

Magnetic Design
18-phase Inverter Supply
Verification Measurements

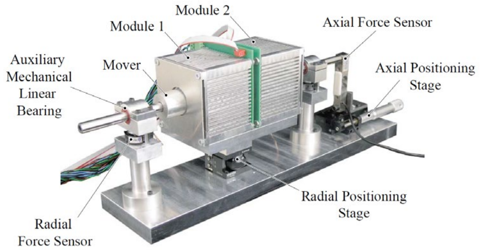

Stator Design

- Choice of the tooth width τ_t and the tooth depth r_t → considering drive, bearing, pull forces
- Scenario for the pull force calculation → the mover sitting on the touch-down bearing (start-up of the MBs)

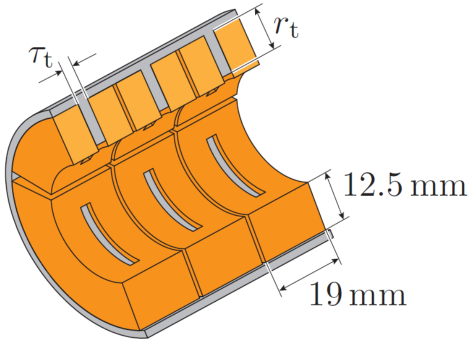

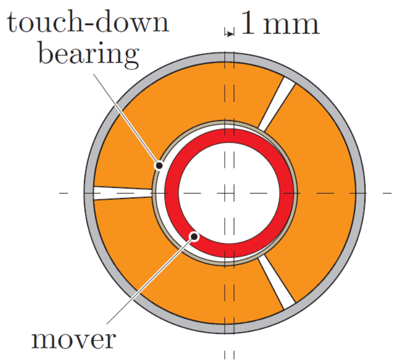

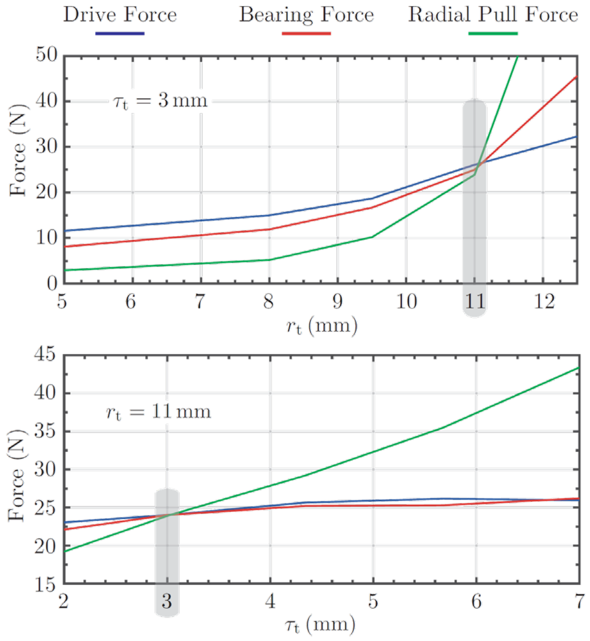

$\tau_t = 3$ mm

$r_t = 11$ mm

- The drive and the bearing forces → obtained for the maximally possible continuous copper losses
- Geometry parameters τ_t and r_t → chosen such that the pull force is lower than the bearing force

[ref] Mirić, Spasoje, et al. "Design and experimental analysis of a new magnetically levitated tubular linear actuator." IEEE Transactions on Industrial Electronics 66.6 (2018): 4816-4825.

Mover Design

- Two mover types considered → surface-mounted PMs (SPM) and interior PMs (IPM)
- First step → parameter range calculated using scaling laws

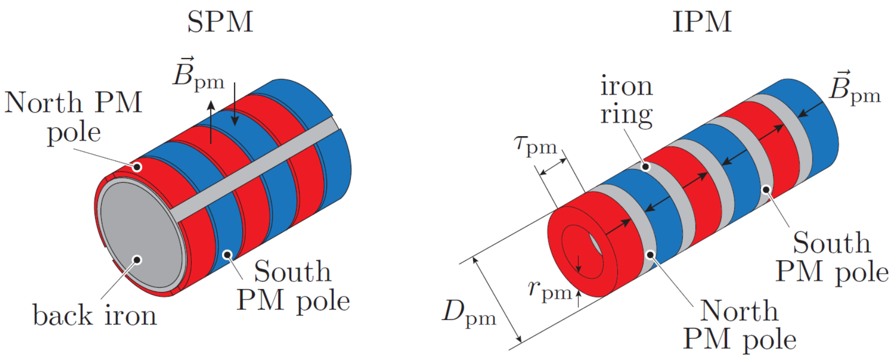

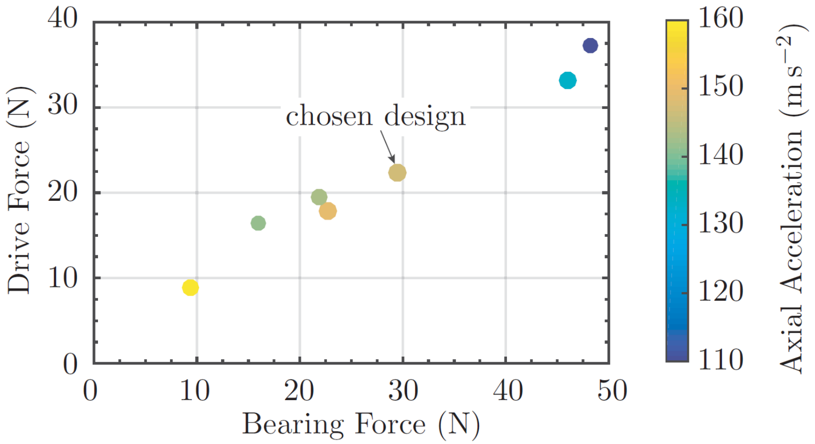

- PM geometry range from the scaling law:

$$\frac{D_{pm} + 2r_{ag}}{D - 2r_{bi}} = [0.5, 0.7] \qquad D_{pm} = (D - 2r_{bi}) \cdot [0.5, 0.7] - 2r_{ag} = [24\text{ mm}, 35.2\text{ mm}]$$

- Final geometry parameters obtained by 3D-FEM:

$$\tau_{pp} = 30\text{ mm} \quad \tau_{pm} = 10\text{ mm} \quad D_{pm} = 27\text{ mm} \quad r_{pm} = 3\text{ mm}$$

- Compromize between performance parameters → drive / bearing forces and axial (linear) acceleration
- The chosen IPM design → axially magnetized PMs and iron rings allow for simplified manufacturing

[ref] Spasoje Miric, 'Linear-Rotary Bearingless Actuators,', PhD Thesis, ETH Zurich, 2021.

Eddy Current Losses

- Short stroke linear actuator → average/max. speed of the mover low to induce eddy current losses
- Solid iron used for the core design → final design check for the eddy current losses

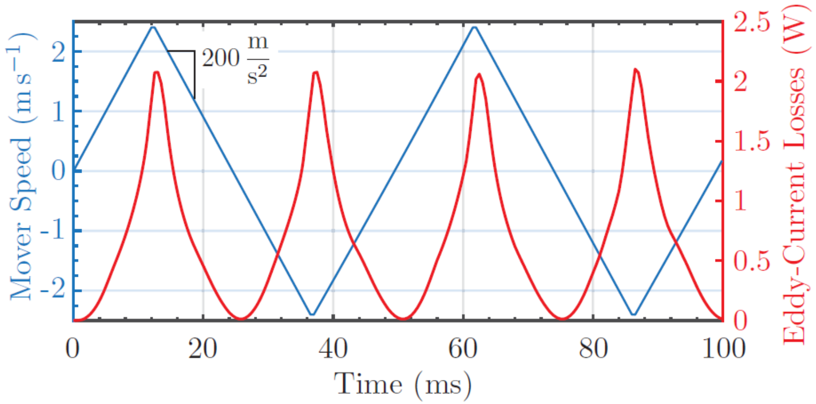

Maximum expected operation conditions:
$20g$ acceleration
$30\ \mathrm{mm}$ stroke

- Average eddy current losses during the operation $= 0.7\ \mathrm{W}$ → 4.7% of the allowed copper losses
- Long stroke actuators that achieve higher speeds → should use low loss core, e.g., soft magnetic composite (SMC)

[ref] Mirić, Spasoje, Dominik Bortis, and Johann Walter Kolar. "Design and comparison of permanent magnet self-bearing linear-rotary actuators." 2019 12th International Symposium on Linear Drives for Industry Applications (LDIA). IEEE, 2019.
[ref] Jensen, William R., Thang Q. Pham, and Shanelle N. Foster. "Linear permanent magnet synchronous machine for high acceleration applications." 2017 IEEE International Electric Machines and Drives Conference (IEMDC). IEEE, 2017.

MALTA Hardware Prototype

- Mover's conductive sleeve → mechanical protection & eddy current position sensing
- Test bench with positioning stages and force sensors → machine constant measurements

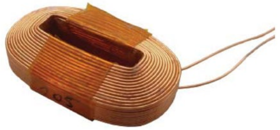

205 turns
0.6 electrical fill factor
0.5 mm wire diameter

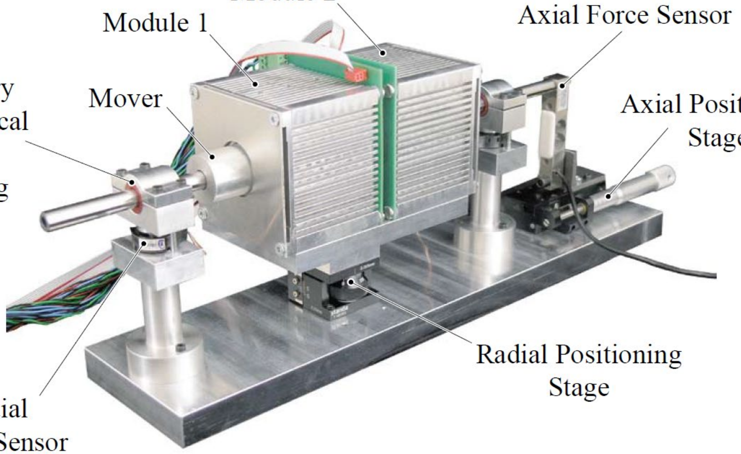

Measurements:

▼ Thermal	▼ Magnetic
$R_{th} = 1.51\ \mathrm{K/W}$	$\hat{\Psi}_M = 8.5\ \mathrm{mWb}$
$\tau_{th} \approx 30\ \mathrm{min}$	$K_D = 7.6\ \mathrm{N/A}$
	$K_B = 5.9\ \mathrm{N/A}$

MALTA Inverter Supply

- **Specifications**
  - 24 phases (8×3 phase)
  - DC link voltage: 45 V
  - DC link capacitance: 4×22 mF (buffer braking energy)
  - Power Semi.: 80 V, 10 A, 15 mΩ
  - $2 \times$ position sensor interfaces
  - Control Board: ZYNQ, Z-7020 (156 digital IOs)

  Current measurement:

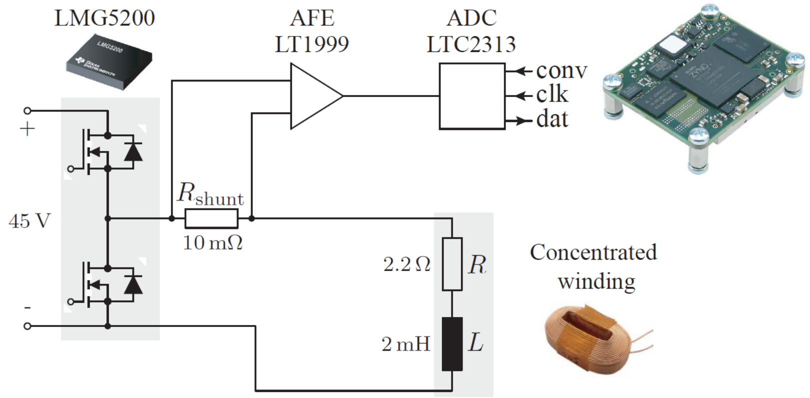

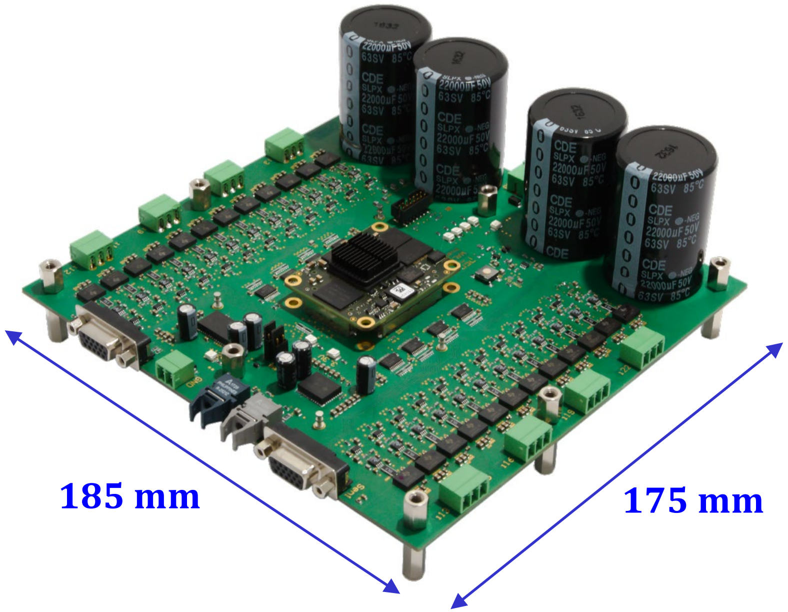

MALTA Hardware Prototype Measurements

- **Measurements: flux linkage, force constants, thermal resistance → prototype characterization/model verification**

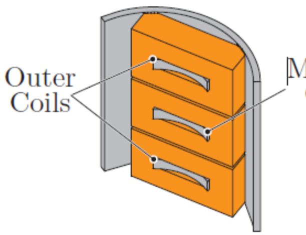

Flux Linkage

	Simulation (mWb)	Measurement (mWb)
Outer Coils:	8.3	8.35
Middle Coil:	9.0	8.85

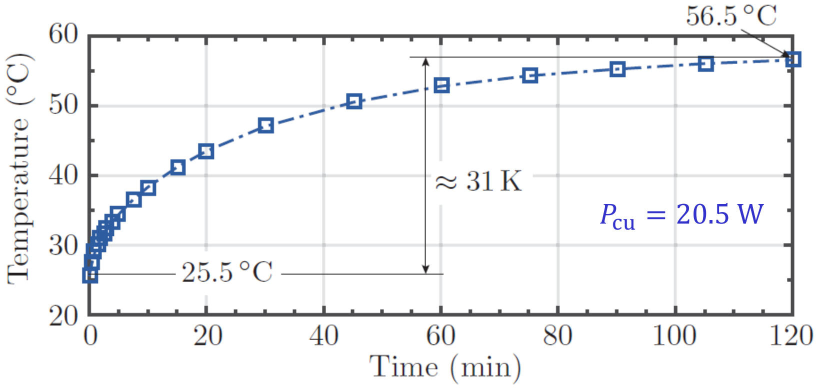

▼ **Magnetic**

$\hat{\Psi}_M = 8.5$ mWb

$K_D = 7.6$ N/A

$K_B = 5.9$ N/A

▼ **Thermal**

$R_{th} = 1.51$ K/W

$\tau_{th} \approx 30$ min

- **Flux linkage measurement → measure induced back EMF and integrate to get the flux linkage**
- **Force constant measurement → apply known current and read the force sensor**
- **R_{th} measurement (winding hot spot to ambient) → apply known losses and read the built-in NTC temp. sensors**

Bearing Force Constant, Decoupling of Bearing and Drive Forces

- Dependence on the rotary angle → measured and simulated with 3D-FEM (saved in a lookup table for control implem.)

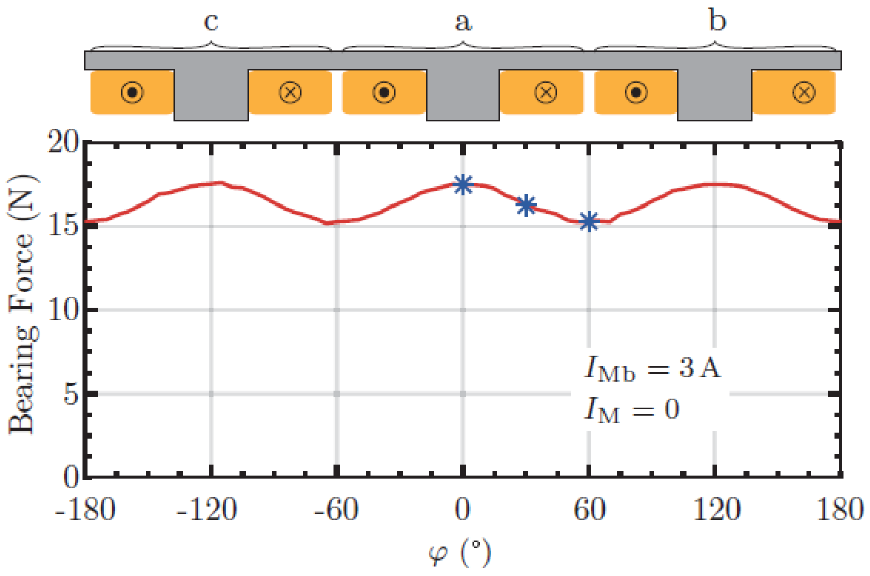

$K_B = 5.9$ N/A, measured range $[5.6\ \mathrm{N/A} - 6.26\ \mathrm{N/A}]$

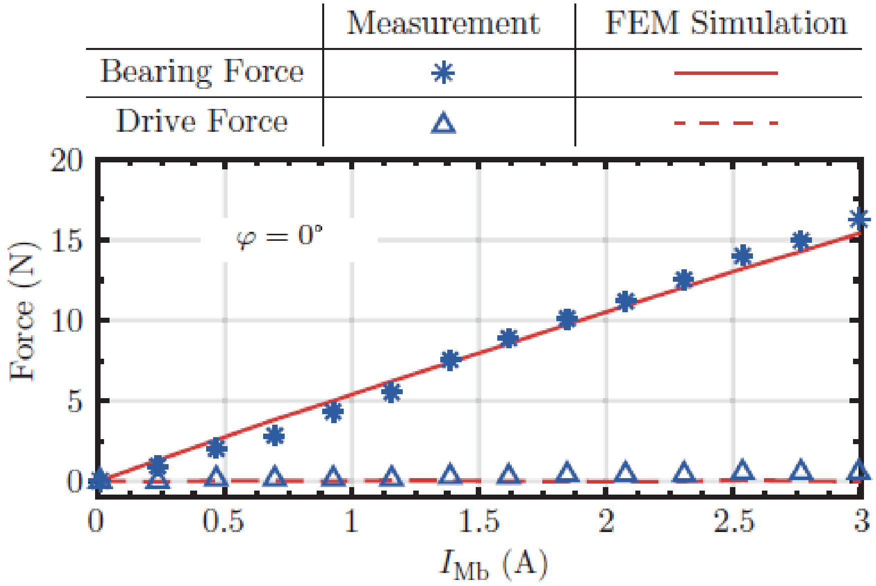

Decoupling of the bearing and the drive force generation!

Attraction/Pull Constant K_A (Pull Force)

- Extremely important parameter for the control system design and implementation
- K_A (also K_{pull}) determines poles of the mechanical dynamic model of the mover

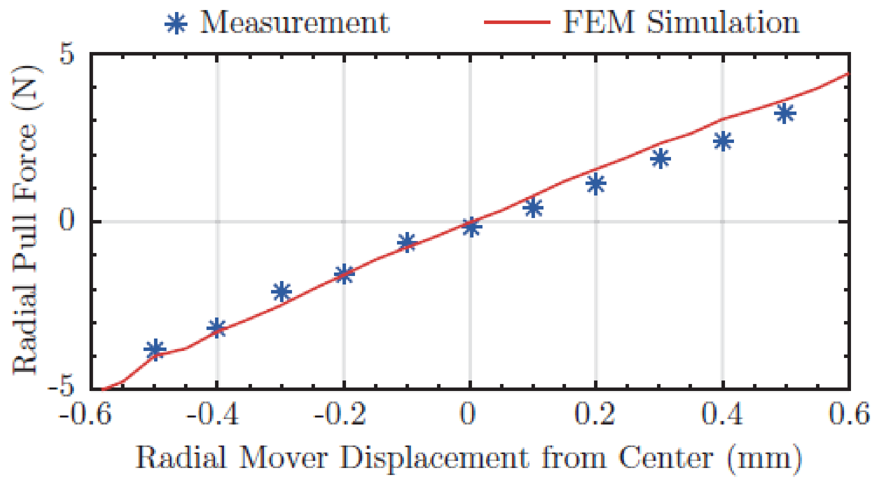

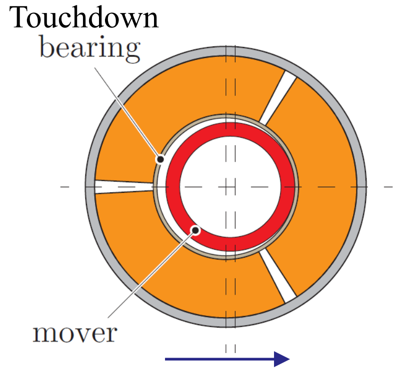

$$K_A = 8.33\ N/\mathrm{mm}$$

- K_A obtained by displacing the mover in radial direction and measuring pull force, with no currents in the winding

Position Sensor

Operating Principle
Driving Electronics
Geometry Optimization

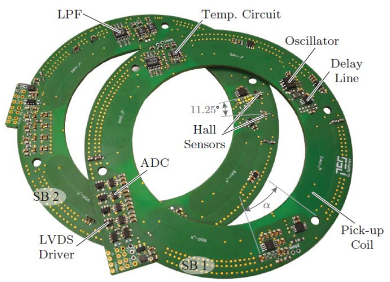

Position Sensing – Linear & Radial

- Sensing locations at the axial ends of the actuator → SP1 and SP2
- Linear position → Hall-effect-based sensors, displaced $\pi/2$ electrical

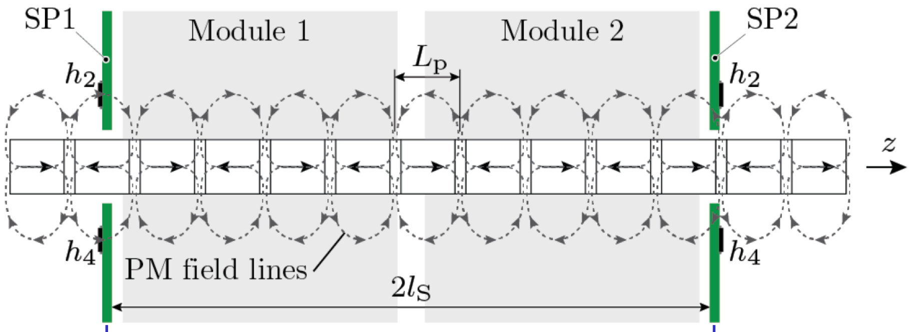

$$h_{\cos} = (h_1 + h_2 + h_3 + h_4)/4$$

$$h_{\sin} = (h_1 + h_2 + h_3 + h_4)/4$$

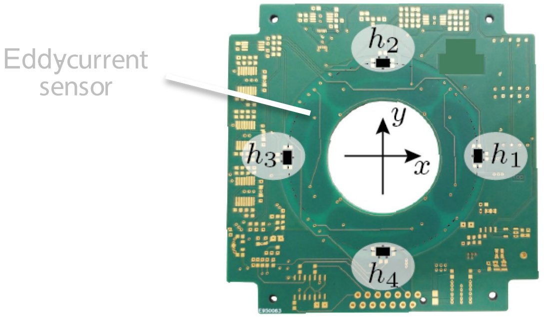

$$\theta_{\mathrm{el}} = \mathrm{atan2}(h_{\sin}, h_{\cos})$$

Axial/Linear Position:

$$z = \frac{L_\mathrm{p}}{\pi}(\theta_{\mathrm{el}} + k \cdot 2\pi)$$

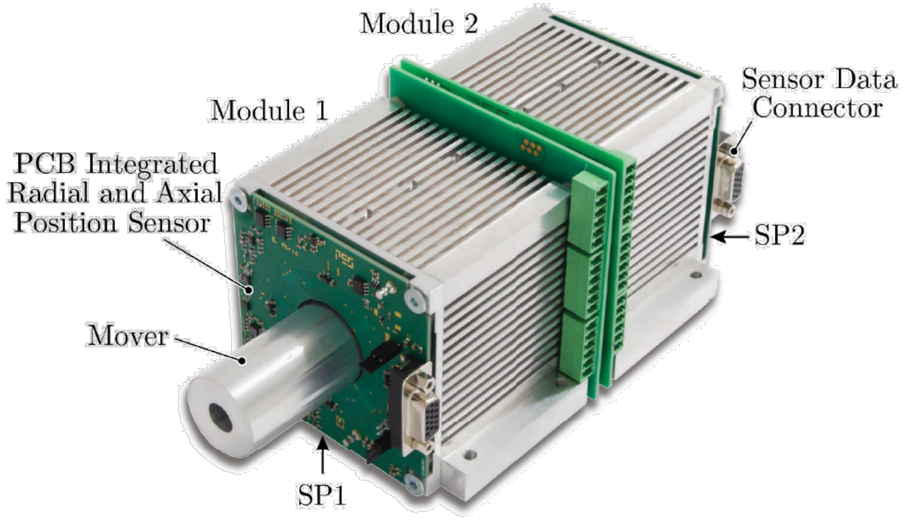

- Radial position sensor → eddy-current based; conductive mover surface is a sensing target
- Advanced eddy-current sensing techniques → later in the tutorial, blood pump part

Eddy-Current Based Position Sensor

- Injection coil carries high-frequency current → induce voltage in pick-up coils
- Upper limit for the oscillation frequency → resonant frequency of the sensor (layout/size dependent)

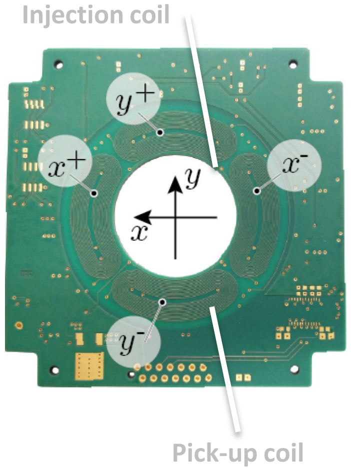

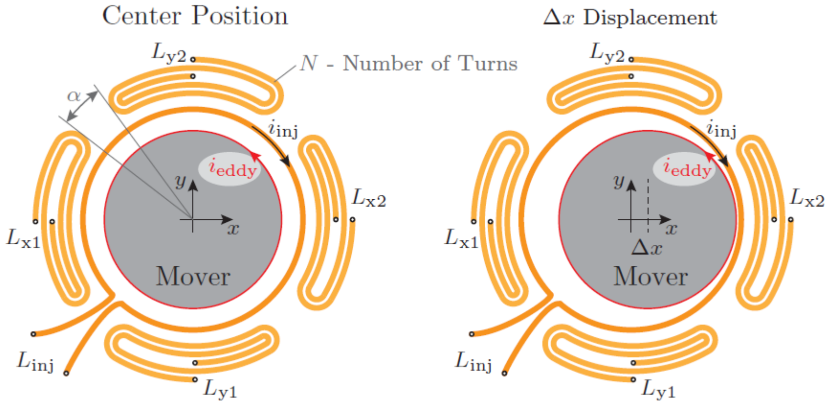

Mutual Inductances:

$M_{\text{inj-x1}} = M_0$
$M_{\text{inj-x2}} = M_0$
$M_{\text{inj-y1}} = M_0$
$M_{\text{inj-y2}} = M_0$

Mutual Inductances:

$M_{\text{inj-x1}} > M_0$
$M_{\text{inj-x2}} < M_0$
$M_{\text{inj-y1}} = M_0$
$M_{\text{inj-y2}} = M_0$

$$i_{\text{inj}} = \hat{I}_{\text{inj}} \sin(\omega_{\text{osc}} t)$$

$$\omega_{\text{osc}} \approx 3 \text{ MHz}, \ \hat{I}_{\text{inj}} \approx 100 \text{ mA}$$

$$M_{\text{inj-x1}} = M_0 + \frac{\partial M_{\text{inj-x1}}}{\partial x} \Delta x$$

$$M_{\text{inj-x2}} = M_0 + \frac{\partial M_{\text{inj-x2}}}{\partial x} \Delta x$$

$$M_{\text{inj-y1}} = M_0 + \frac{\partial M_{\text{inj-y1}}}{\partial y} \Delta y ,$$

$$M_{\text{inj-y2}} = M_0 + \frac{\partial M_{\text{inj-y2}}}{\partial y} \Delta y$$

- Anti-series connection of pick-up coils of the same axis → $(L_{x1} \leftrightarrow L_{x2})$ and $(L_{y1} \leftrightarrow L_{y2})$
- At center position ind. voltage of anti-series connection is zero; it is non-zero if there is mover displacement

Eddy-Current Sensor Electronics

- $x-$ axis example → the induced voltage Δe_{x} rectified and low-pass filtered results in U_{x}
- The same electrical circuit is employed for the $y-$ axis

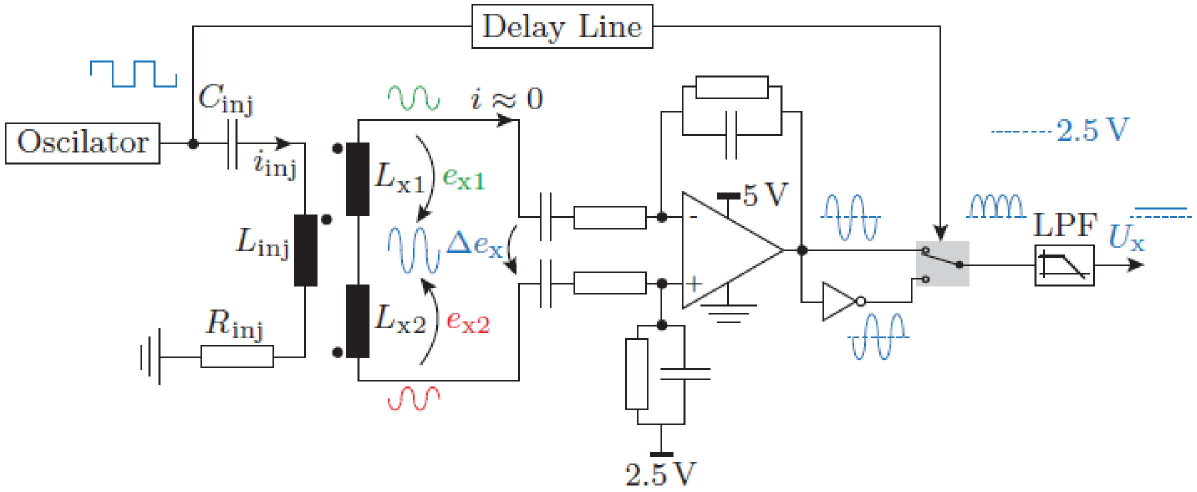

$$U_{\mathrm{x}} \sim 2\omega_{\mathrm{osc}}\, \hat{I}_{\mathrm{inj}} \frac{\partial M}{\partial r} \Delta x.$$

$\omega_{\mathrm{osc}} \approx 3$ MHz, $\hat{I}_{\mathrm{inj}} \approx 100$ mA

- Eddy-current position sensor processing electronics

- $\partial M / \partial r$ inductance sensitivity with radial displacement → maximized by the sensor geometry optimization
- Oscillation frequency ω_{osc} limited by the resonance; injection current i_{inj} limited by the oscillator power

Eddy-Current Sensor Geometry Optimization

- Optimization parameters → angle between the pick-up coils α and the number of turns N of the pick-up coils
- Maximize sensitivity about the radial displacements of the mover → $\partial M/\partial r$

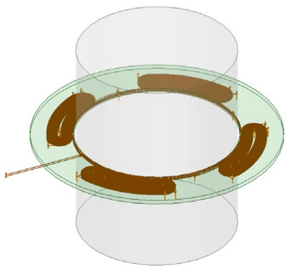

- Model in Ansys Q3D

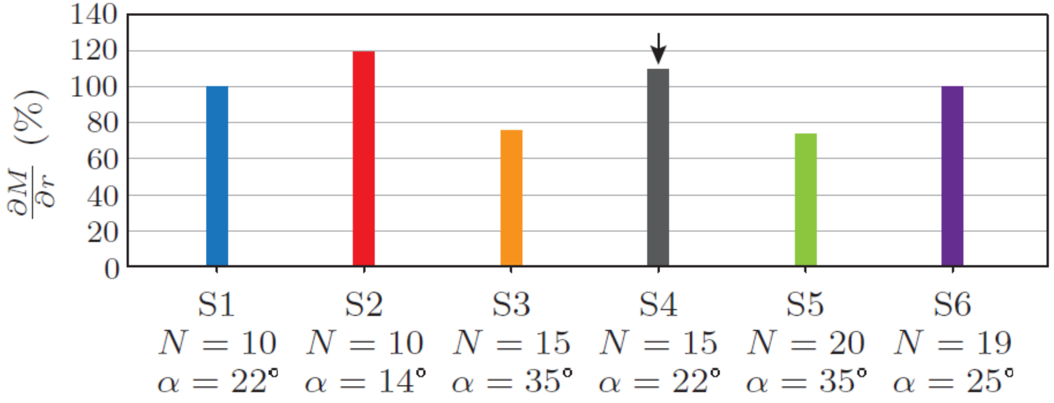

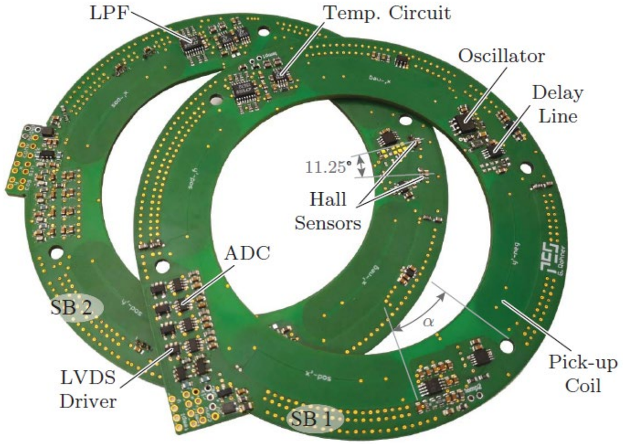

- Optimum number of turns N → larger N does means larger size of the pick-up coil
- Reasonable angle α → leave space for the signal processing electronics (analog circuits & ADCs)

universität innsbruck

Dynamic Modeling

Dynamic Model Derivation
Model Analysis
Relative Gain Array

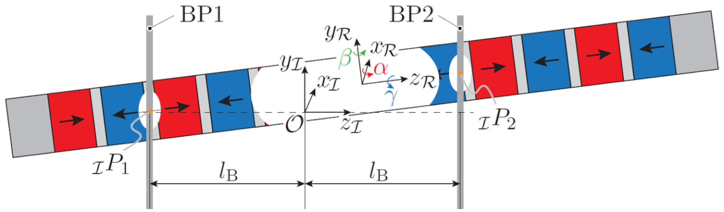

innsbruck Drive and Energy Systems Laboratory

Controller Structure

- Linear motion, radial position and tilting of the mover should be controlled
- Interaction (force action) points between the stator and the mover → middle of the stator (module)

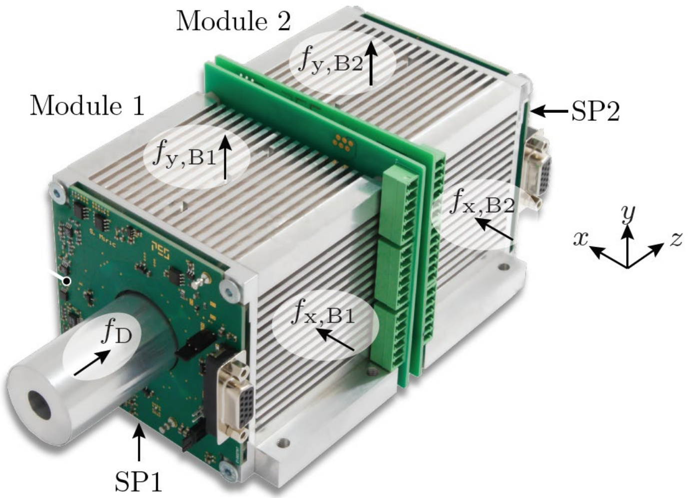

- Control plant

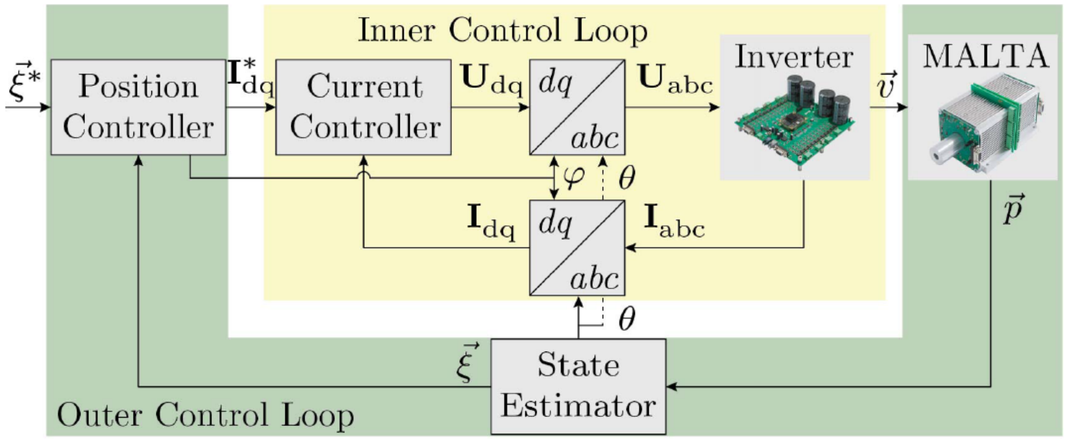

- Controller structure

- Cascaded controller structure → outer position controller (slow) and inner current control loop (fast)
- Dynamic modelling of the plant → electrical model, mechanical model, position sensor model

[ref] Mirić, Spasoje, et al. "Dynamic electromechanical model and position controller design of a new high-precision self-bearing linear actuator." IEEE Transactions on Industrial Electronics 68.1 (2020): 744-755.

Dynamic Models for Controller Design

- Dynamic models necessary for the controller design → electric, mechanical, position sensor model
- Electric model → $abcdq$ transformation of the phase quantities; dq currents control forces on the mover

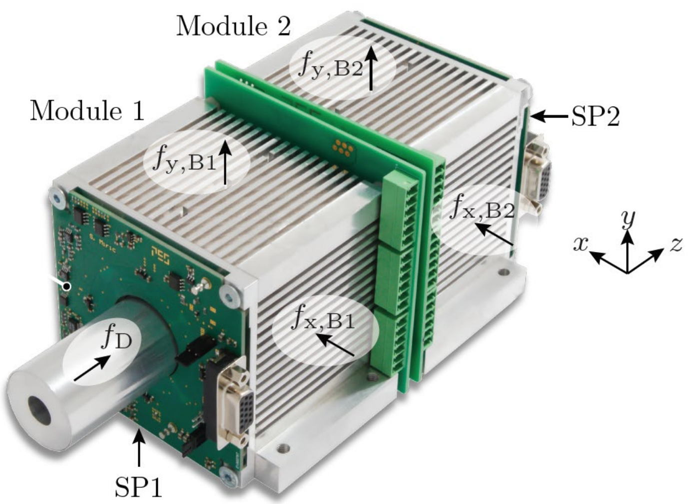

- Control plant

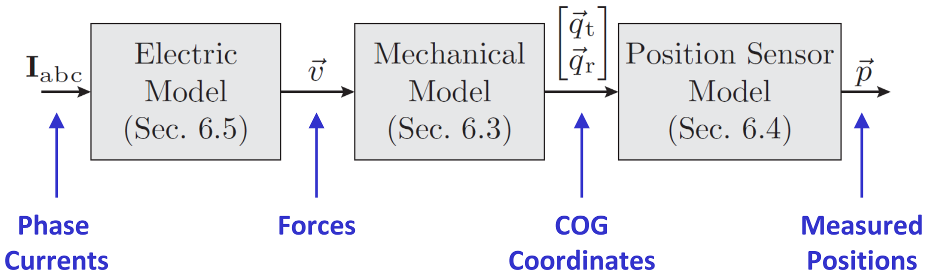

$$\mathbf{I}_{\mathrm{abc}} = \begin{bmatrix} i_{\mathrm{aA}} & i_{\mathrm{aB}} & i_{\mathrm{aC}} \\ i_{\mathrm{bA}} & i_{\mathrm{bB}} & i_{\mathrm{bC}} \\ i_{\mathrm{cA}} & i_{\mathrm{cB}} & i_{\mathrm{cC}} \end{bmatrix} \qquad \vec{v} = \begin{bmatrix} f_{\mathrm{xB1}} \\ f_{\mathrm{yB1}} \\ f_{\mathrm{xB2}} \\ f_{\mathrm{yB2}} \\ f_{\mathrm{zD}} \end{bmatrix} \qquad \vec{q} = \begin{bmatrix} x \\ y \\ z \\ \alpha \\ \beta \\ \gamma \end{bmatrix} \begin{matrix} \} \ \vec{q}_{\mathrm{t}} \\ \\ \} \ \vec{q}_{\mathrm{r}} \end{matrix} \qquad \vec{p} = \begin{bmatrix} x_1 \\ y_1 \\ x_2 \\ y_2 \\ z \end{bmatrix}$$

- Overview of the dynamic models

- Mechanical model → MIMO model, coupling between the axes of motion; equations of motion must be derived
- Position sensor model → mech. model obtains COG coordinates, position sensor measures displacements

[ref] Mirić, Spasoje, et al. "Dynamic electromechanical model and position controller design of a new high-precision self-bearing linear actuator." IEEE Transactions on Industrial Electronics 68.1 (2020): 744-755.

Inertial $\mathcal{I}$ and Rotary $\mathcal{R}$ Reference Frames

- Inertial reference frame → between modules, point $\mathcal{O}$; rotary reference frame → mover's COG, point $\mathcal{O}_{\mathrm{COG}}$
- Position of the rotary RF with respect to inertial RF determines the mover's position

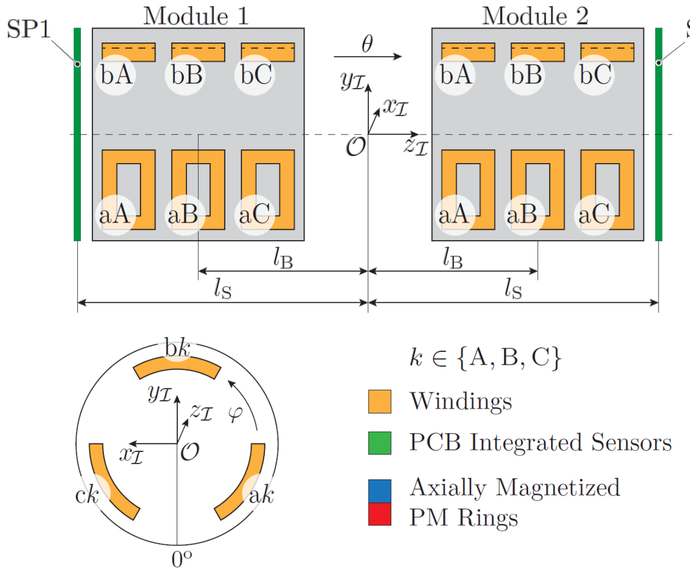

- Inertial reference frame

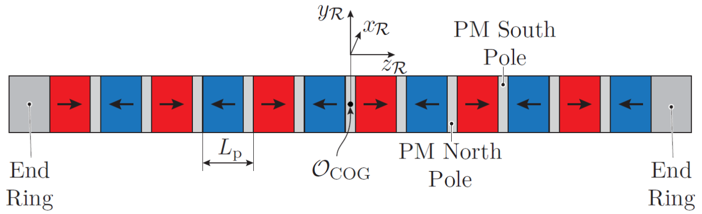

- Rotary reference frame

- l_{B} - the distance between the force action point and $\mathcal{O}$; l_{S} - the distance of the position sensors
- Electrical angles → θ – linear electrical angle; φ – rotary electrical angle (bearing force direction)

[ref] Mirić, Spasoje, et al. "Dynamic electromechanical model and position controller design of a new high-precision self-bearing linear actuator." IEEE Transactions on Industrial Electronics 68.1 (2020): 744-755.

Equations of Motion (EoM)

- Newton-Euler equations of motion → equation of motion in IRF (1) and rotation equation in RRF (2)
- Interaction points $_{\mathcal{I}}P_1$ and $_{\mathcal{I}}P_2$ → center of the stator (module)

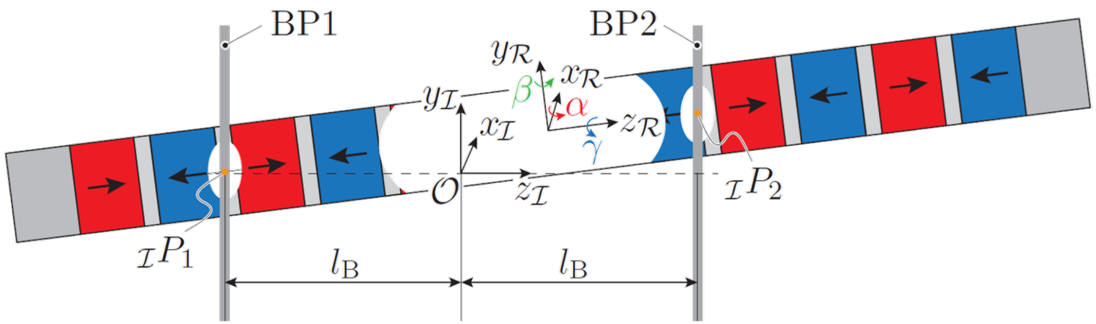

$$\vec{q}_{\mathrm{t}} = \begin{bmatrix} x \\ y \\ z \end{bmatrix} \qquad \vec{q}_{\mathrm{r}} = \begin{bmatrix} \alpha \\ \beta \\ \gamma \end{bmatrix}$$

$$m\frac{\partial^2 \vec{q}_{\mathrm{t}}}{\partial t^2} = {}_{\mathcal{I}}\vec{F}_{\mathrm{tot}} \qquad (1)$$

$${}_{\mathcal{R}}\mathbf{I}_{\mathrm{m}} \cdot \frac{\partial_{\mathcal{R}}\vec{\omega}}{\partial t} + {}_{\mathcal{R}}\vec{\omega} \times {}_{\mathcal{R}}\mathbf{I}_{\mathrm{m}} \cdot {}_{\mathcal{R}}\vec{\omega} = {}_{\mathcal{R}}\vec{T}_{\mathrm{tot}}, \qquad (2)$$

m - mass of the mover
$_{\mathcal{R}}\mathbf{I}_{\mathrm{m}}$ - MoI of the mover

IRF - inertial reference frame
RRF - rotary reference frame

$${}_{\mathcal{R}}\mathbf{I}_{\mathrm{m}} = \begin{bmatrix} I_{xx} & 0 & 0 \\ 0 & I_{yy} & 0 \\ 0 & 0 & I_{zz} \end{bmatrix}$$

- Cardan (Euler) angles α, β, γ → mover's rotation around respective axes $x_{\mathcal{I}}, y_{\mathcal{I}}, z_{\mathcal{I}}$
- In total 6 equations → 3 for linear motion and 3 for rotation

[ref] Mirić, Spasoje, et al. "Dynamic electromechanical model and position controller design of a new high-precision self-bearing linear actuator." IEEE Transactions on Industrial Electronics 68.1 (2020): 744-755.

Position Control Bandwidth, SISO or MIMO Controller

- Eigenvalues of the matrix A → determine the dynamics of the systems and the minimum required bandwidth
- Closed-loop position controller bandwidth → should be at least twice the maximum unstable pole

Symbol	Mode	Eigenvalue
$\lambda_{1,2}$	x	$\pm 218.92\,\mathrm{rad\,s^{-1}}$
$\lambda_{3,4}$	y	$\pm 218.92\,\mathrm{rad\,s^{-1}}$
$\lambda_{5,6}$	z	$\pm 0.9893\,\mathrm{rad\,s^{-1}}$
$\lambda_{7,8}$	α	$\pm 157.53\,\mathrm{rad\,s^{-1}}$
$\lambda_{9,10}$	β	$\pm 157.53\,\mathrm{rad\,s^{-1}}$

- Eigenvalues of the matrix A

$$G_{ij}(s) = \mathbf{C}_i \cdot (s\mathbf{I} - \mathbf{A})^{-1} \cdot \mathbf{B}_j \Rightarrow$$

$$\Lambda(G(s)) \mathrel{\widehat{=}} G(s) \times \left(G(s)^{-1}\right)^{\top}$$

$$\text{RGA-number}(G(s)) = \|\Lambda(G(s)) - I_{Pair}\|_{Sum}$$

$$\begin{aligned}\omega_c &= 2 \times \max\left(|\lambda_{\{1,2,3,4,5,6,7,8,9,10\}}|\right)\\ &= 2 \times 218.92\,\mathrm{rad\,s^{-1}}\\ &= 436\,\mathrm{rad\,s^{-1}}.\end{aligned}$$

- Minimum closed-loop bandwidth of the position controller

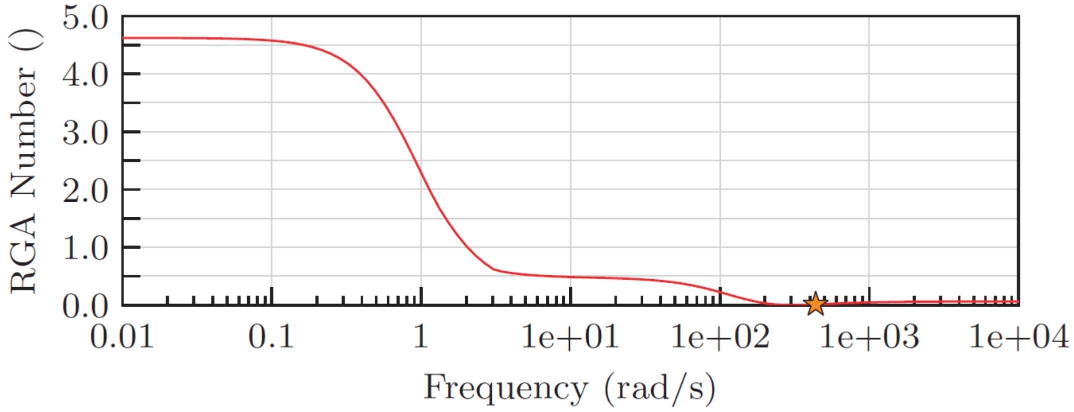

- RGA number

- RGA number → helps to identify the level of coupling between the input and outputs of the system
- Low RGA number → low coupling and SISO control possible

[ref] Mirić, Spasoje, et al. "Dynamic electromechanical model and position controller design of a new high-precision self-bearing linear actuator." IEEE Transactions on Industrial Electronics 68.1 (2020): 744-755.

universität innsbruck

Controller Design

MIMO and SISO Controllers
Measurement Results
Tilting Control Example

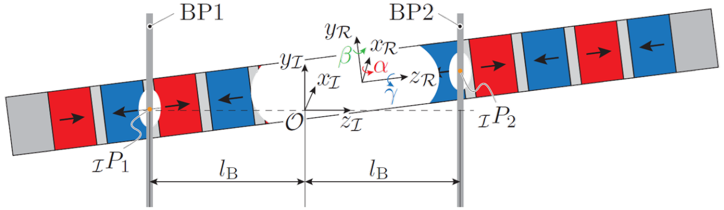

MIMO Controller

- **Cascaded Control Structure**
  - Outer Loop: Position Control (BW: 60 Hz)
  - Inner Loop: Current Control (BW: 470 Hz)

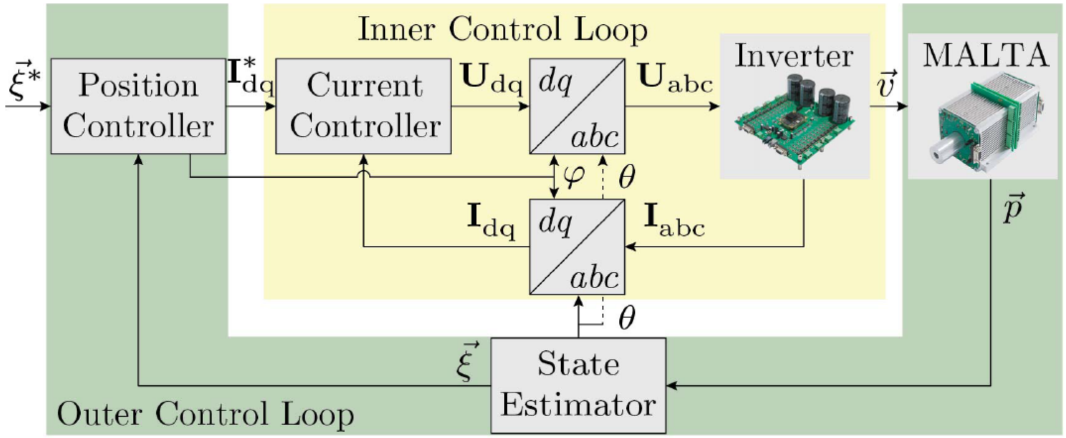

- Position Controller Tuning: LQG
- (MALTA – Magnetically Levitated Tubular Actuator)

- **Position Controller Structure ($\vec{\xi}_{\mathrm{aug,pu}} \in \mathbb{R}^{15}$)**

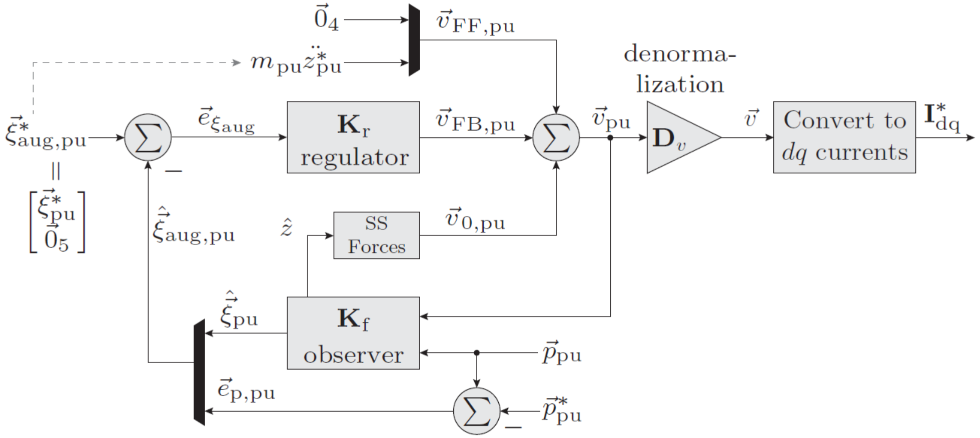

- **Current Controller Structure ($\mathbf{I}_{\mathbf{dq}} \in \mathbb{R}^{4\times4}$)**

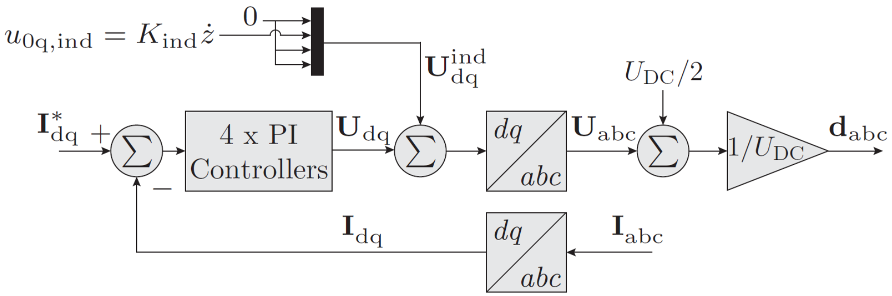

[ref] Mirić, Spasoje, et al. "Dynamic electromechanical model and position controller design of a new high-precision self-bearing linear actuator." IEEE Transactions on Industrial Electronics 68.1 (2020): 744-755.

SISO Controller (1)

- Separated winding example
- xy bearing winding

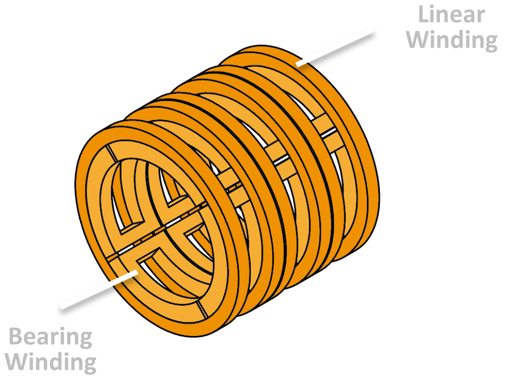

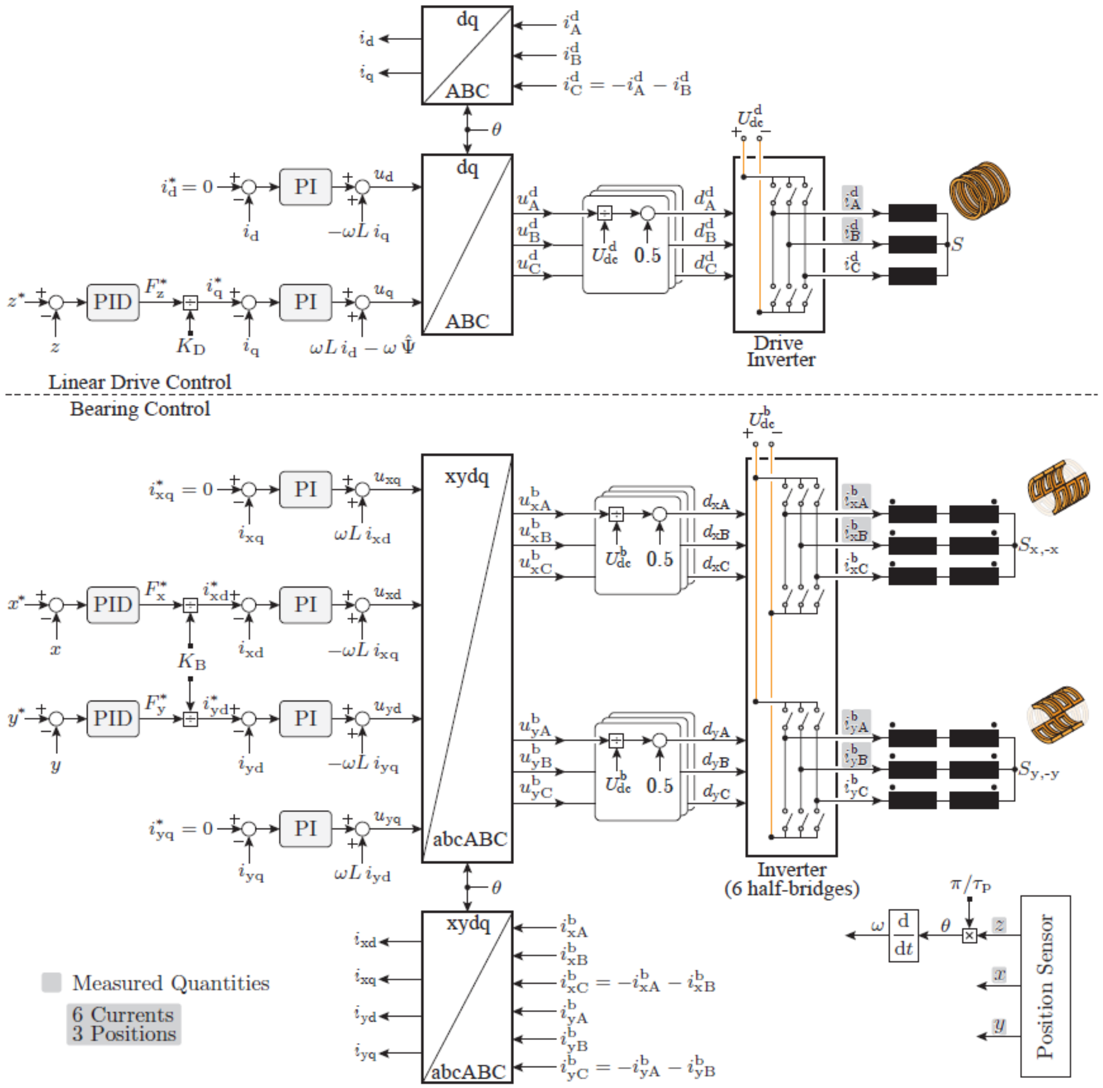

- Linear & bearing controller separated
- Bearing windings in anti-series conn.

[ref] Mirić, Spasoje, Dominik Bortis, and Johann Walter Kolar. "Design and comparison of permanent magnet self-bearing linear-rotary actuators." 2019 12th International Symposium on Linear Drives for Industry Applications (LDIA). IEEE, 2019.

SISO Controller (2)

- Combined winding example
- $abcABC$ winding

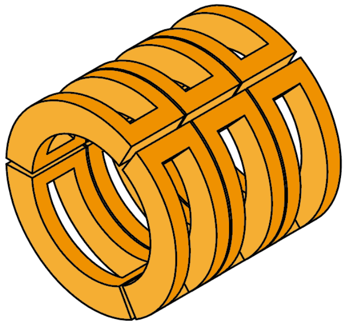

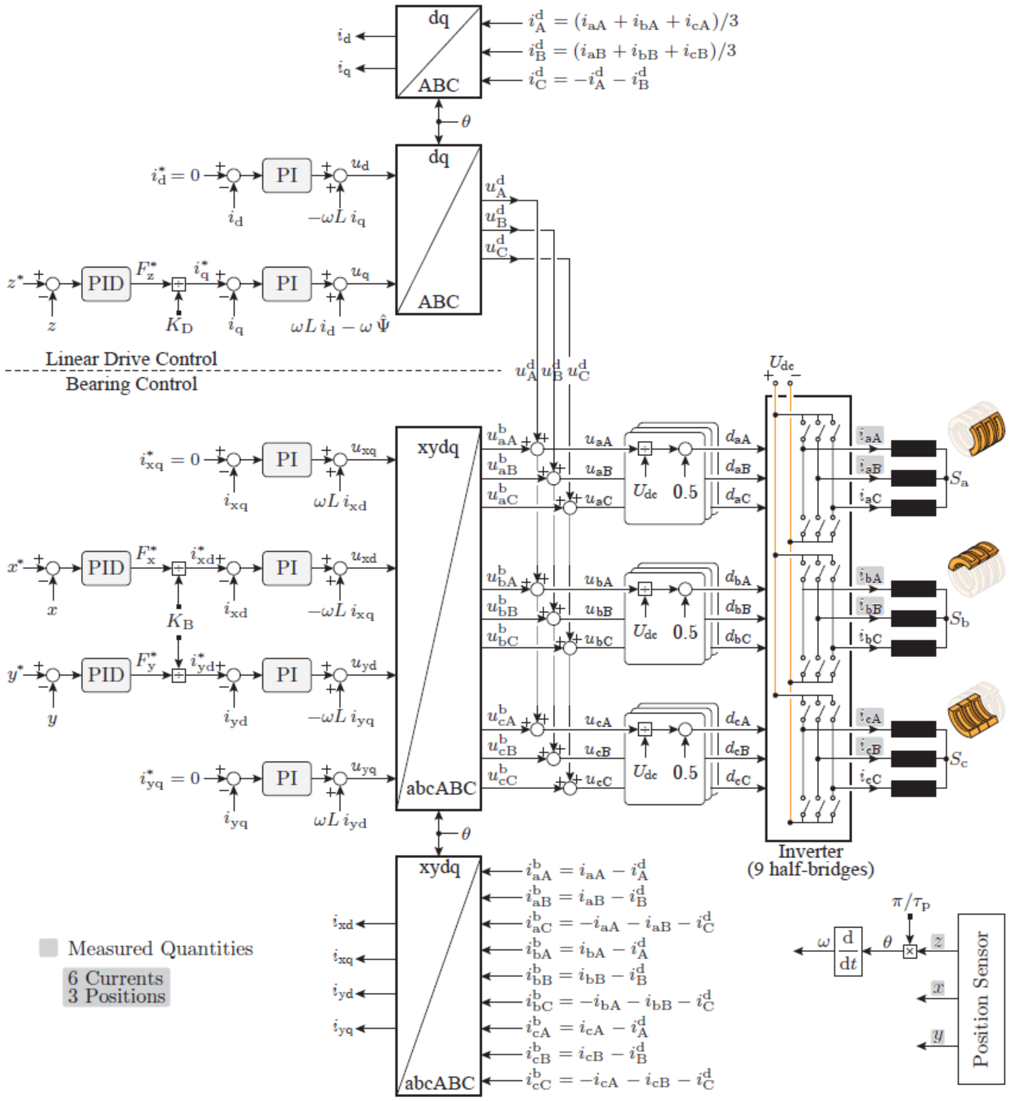

- Superimpose control signals
- 3 three-phase systems in linear dir.

[ref] Mirić, Spasoje, Dominik Bortis, and Johann Walter Kolar. "Design and comparison of permanent magnet self-bearing linear-rotary actuators." 2019 12th International Symposium on Linear Drives for Industry Applications (LDIA). IEEE, 2019.

MIMO – Measurement Results

■ Axial Reference Tracking

- **Axial Position and Force**

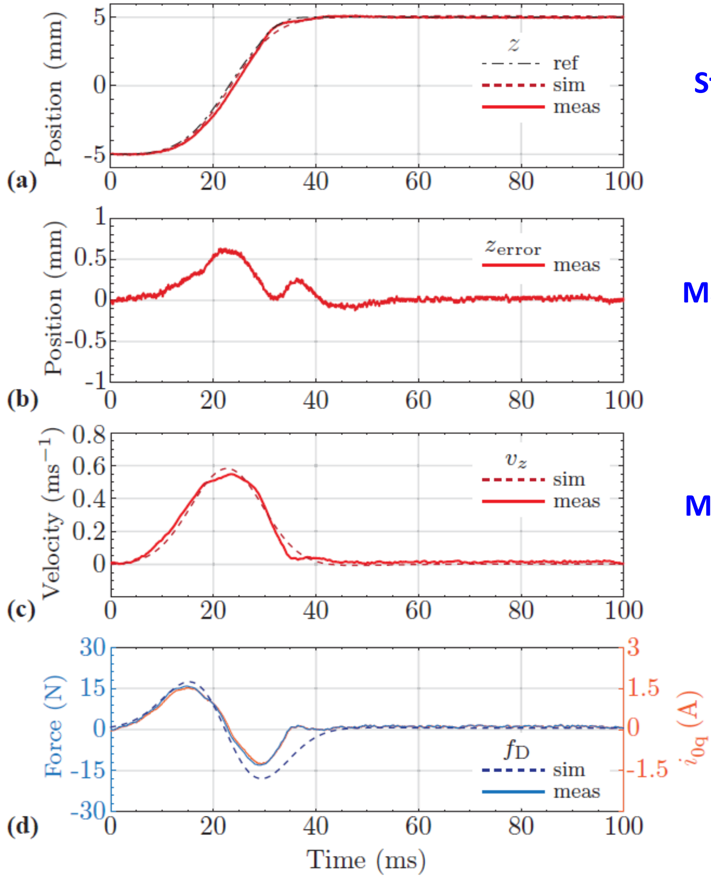

Stroke: 10 mm

Max. Pos. Error: 0.5 mm

Max. Speed: 0.6 m/s

Axial Force:
± 15 N

- **Radial Position and Force**

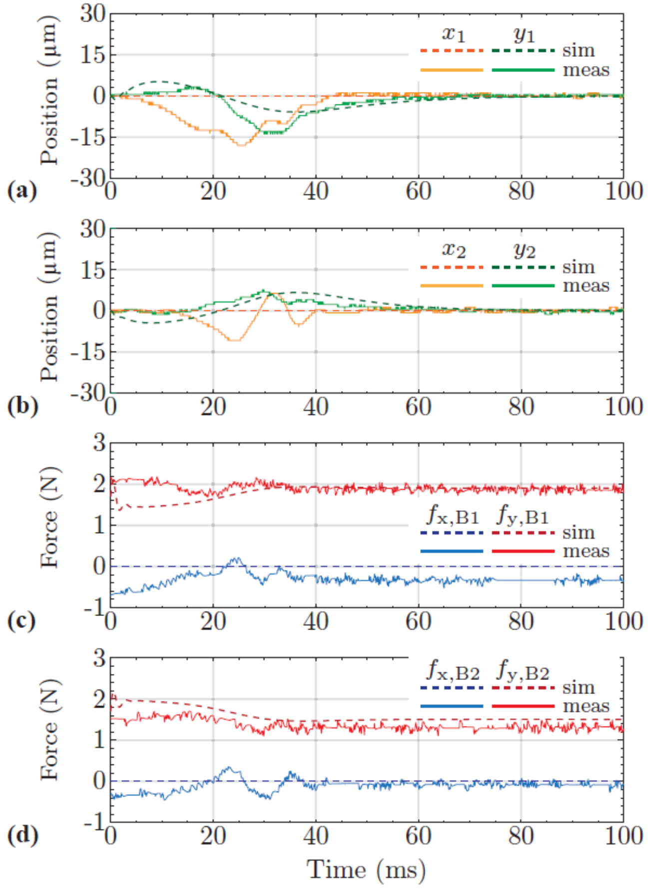

Max. Radial
Position Oscillation (1.5%):
± 15 µm

Mechanical Air Gap
± 1000 µm

Y-direction
Compensates
Gravity Force:
3.25 N

MIMO – Measurement Results

■ Steady-State Positioning

- Sensor Resolution ~1 µm
- Number of Measured Samples: 2000

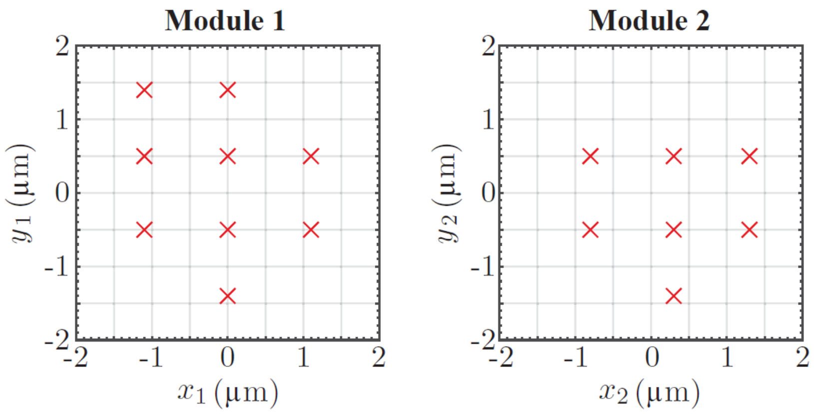

Mean
$\mathrm{mean}(x_1) = 0.0335\ \mu\mathrm{m}$
$\mathrm{mean}(y_1) = -0.0212\ \mu\mathrm{m}$

STD
$\mathrm{std}(x_1) = 0.3883\ \mu\mathrm{m}$
$\mathrm{std}(x_1) = 0.5579\ \mu\mathrm{m}$

Mean
$\mathrm{mean}(x_2) = 0.0579\ \mu\mathrm{m}$
$\mathrm{mean}(y_2) = -0.0735\ \mu\mathrm{m}$

STD
$\mathrm{std}(x_2) = 0.4827\ \mu\mathrm{m}$
$\mathrm{std}(x_2) = 0.4956\ \mu\mathrm{m}$

■ Mover Tilting Control

- High Precision Applications (e.g. Pick-And-Place)
- Thermal Expansions of Parallel Kinematics

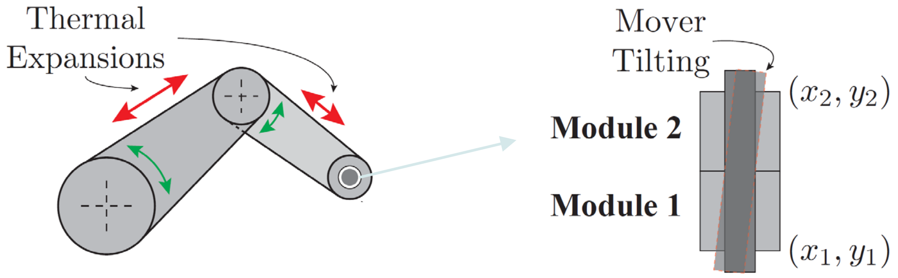

- Tilting Experimental Verification:

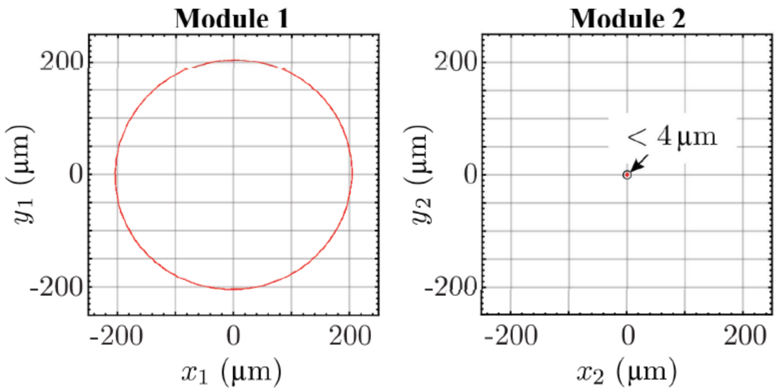

SISO – Measurement Results

- **Oscillatory Operation**

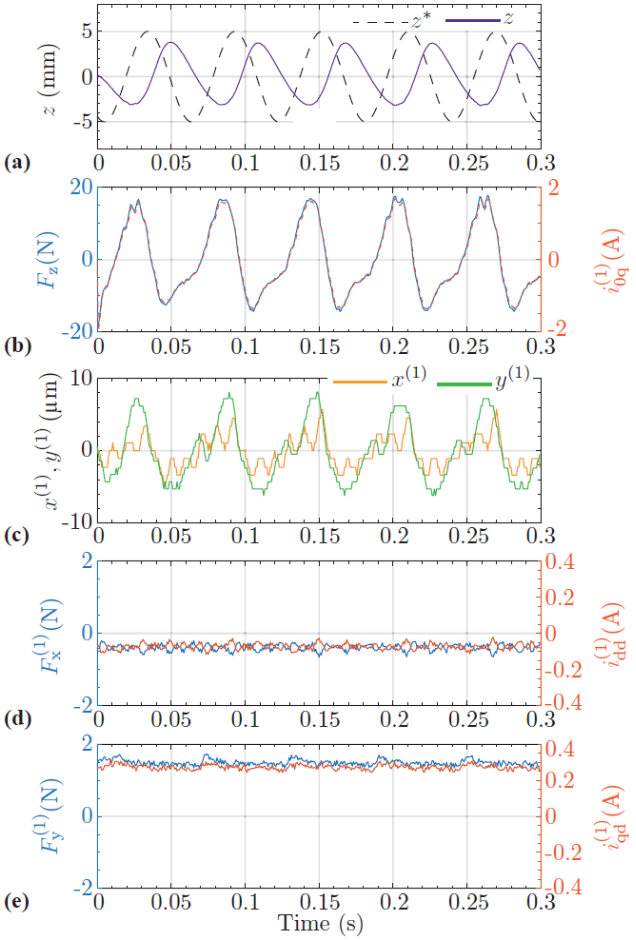

Stroke: 10 mm
Frequency: 17 Hz

Force: $< |\pm 20|$ N

Radial Position: $< |\pm 10|$ µm

- **Axial Sub-plant Bode Plot**
  - **Blue: Analytically Derived Transfer Function**
  - **Red: Experimentally Verified Points: $f_z = \{1, 3, 5, \ldots, 19, 21\}$ Hz**

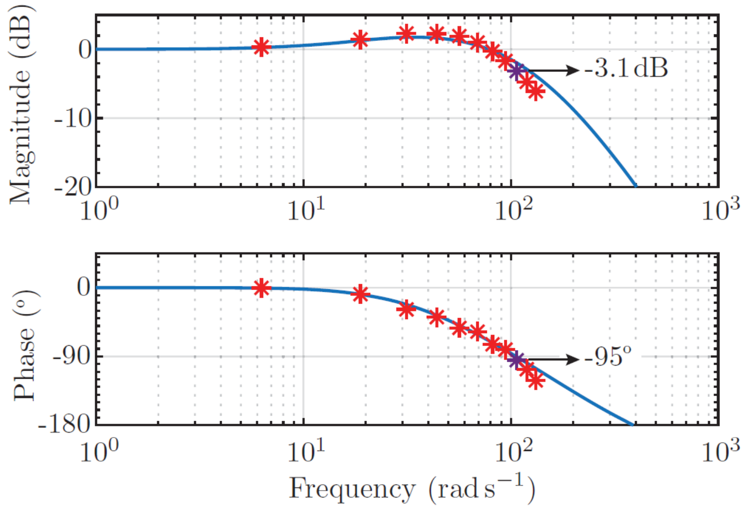

- **Demonstration of the Real Life Operation →**

Linear Bearingless Actuator

- Video (10 Hz, 1 Hz)

universität innsbruck

Generalized Complex Space Vector Modelling

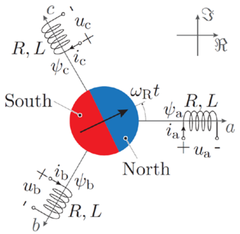

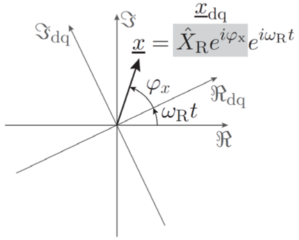

innsbruck Drive and Energy Systems Laboratory

Generic Complex Space Vector Modeling (1)

■ Three-Phase (a, b, c) → Two-Phase (d, q)

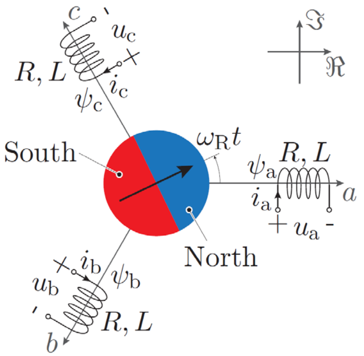

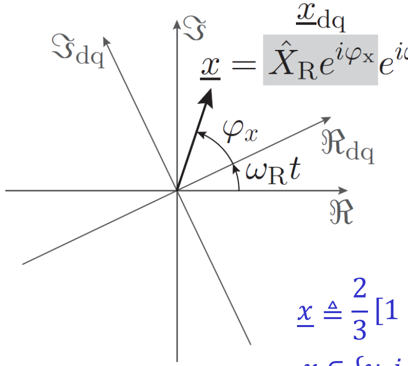

$$\underline{x} = \underbrace{\hat{X}_R e^{i\varphi_x}}_{\underline{x}_{dq}} e^{i\omega_R t}$$

$$\underline{a} = e^{i(2\pi/3)}$$

$$\underline{x} \triangleq \frac{2}{3}\begin{bmatrix} 1 & \underline{a} & \underline{a}^2 \end{bmatrix}\begin{bmatrix} x_a \\ x_b \\ x_c \end{bmatrix}$$

$$x \in \{u, i, \psi\}$$

■ Example: Current Space Vector

▼ Three-phase currents

$$\left.\begin{aligned} i_a &= \hat{I}_R \cdot \cos(\omega_R t + \varphi_i) \\ i_b &= \hat{I}_R \cdot \cos(\omega_R t + \varphi_i - 2\pi/3) \\ i_c &= \hat{I}_R \cdot \cos(\omega_R t + \varphi_i + 2\pi/3) \end{aligned}\right\}$$

▼ Space vector

$$\underline{i} = \underbrace{\hat{I}_R \cdot e^{i\cdot\varphi_i}}_{} \cdot e^{i\cdot\omega_R t}$$

$$\underline{i}_{dq} = \hat{I}_R \cdot e^{i\cdot\varphi_i} = i_d + i \cdot i_q$$

■ Rotary Machine: Torque

▼ Stator: 6 concentrated coils

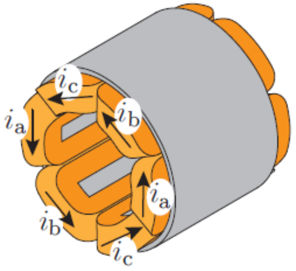

$$\underline{\psi}_{dq} = \hat{\Psi}_R$$

▼ PM Rotor: $N_{pp,R} = 4$

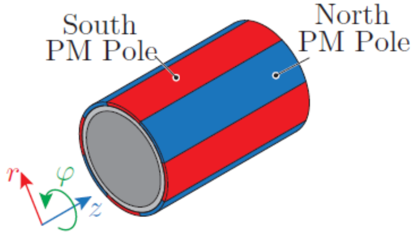

$$\boldsymbol{T_z} = \frac{3}{2} \boldsymbol{N_{pp,R}} \cdot \boldsymbol{\hat{\Psi}_R} \cdot \boldsymbol{i_q}$$

■ Linear Machine: Thrust Force

▼ Stator: 3 concentrated coils

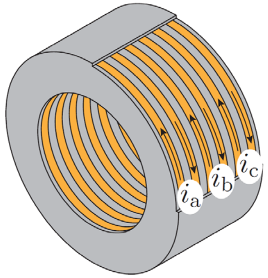

$$\underline{\psi}_{dq} = \hat{\Psi}_L$$

$$\omega_L = \frac{2\pi}{\tau_{pp}} \cdot v_z$$

▼ PM Rotor: 4 poles

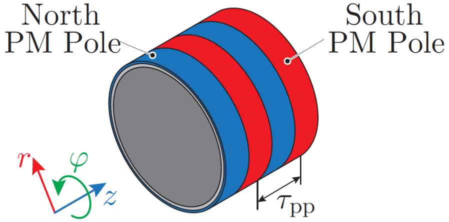

$$\boldsymbol{F_z} = \frac{\boldsymbol{3\pi}}{\boldsymbol{\tau_{pp}}} \cdot \boldsymbol{\hat{\Psi}_L} \cdot \boldsymbol{i_q}$$

Generic Complex Space Vector Modeling (2)

- **Rotary Machine: Bearing Force**

▼ Torque Generation

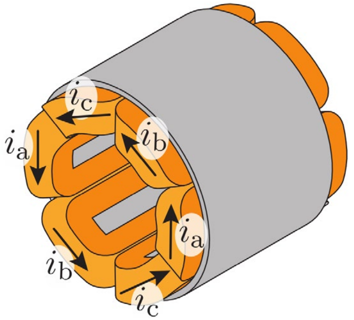

▼ Bearing Force Generation

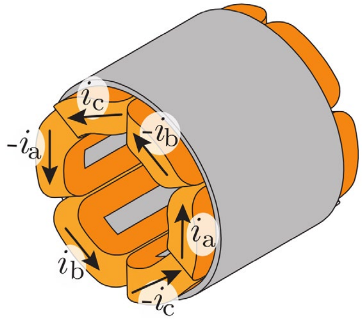

- **Rotor in Center → No Flux Linkage**
  - Model: two coils in anti-series connection

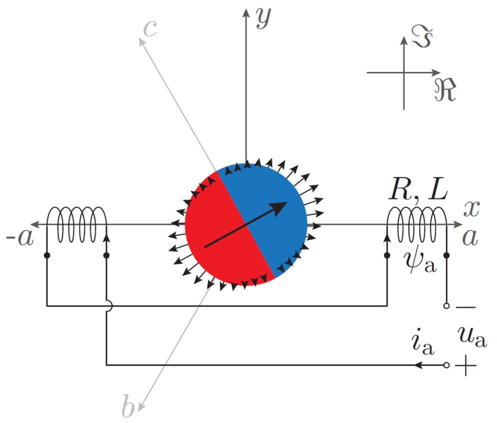

- **Displaced Rotor → $\frac{d\hat{\Psi}_R}{dx} = \frac{d\hat{\Psi}_R}{dy} = \chi_{pm,R}$**
  - Flux linkage radial sensitivity

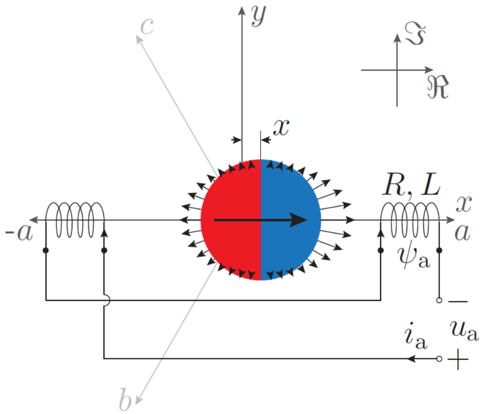

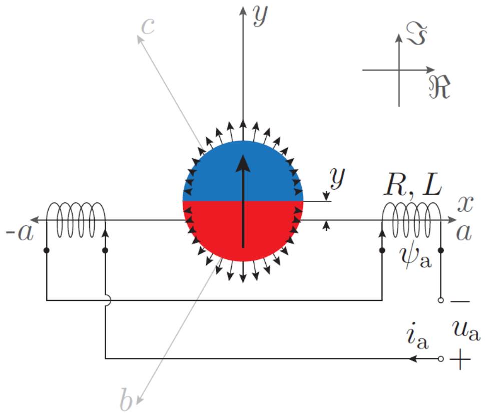

▼ Three Phase Flux Linkage

$$\psi_a = \chi_{pm,R} \cdot [x \cdot \cos(\omega_R t + \varphi_\psi) - y \cdot \sin(\omega_R t + \varphi_\psi)]$$
$$\psi_b = \chi_{pm,R} \cdot [x \cdot \cos(\omega_R t + \varphi_\psi - 2\pi/3) - y \cdot \sin(\omega_R t + \varphi_\psi - 2\pi/3)]$$
$$\psi_c = \chi_{pm,R} \cdot [x \cdot \cos(\omega_R t + \varphi_\psi + 2\pi/3) - y \cdot \sin(\omega_R t + \varphi_\psi + 2\pi/3)]$$

▼ Space Vector

$$\underline{\psi} = \underbrace{\chi_{pm,R} \cdot (x + i \cdot y) \cdot e^{i \cdot \varphi_\psi}}\cdot e^{i \cdot \omega_R t}$$

$$\underline{\psi}_{dq} = \chi_{pm,R} \cdot (x + i \cdot y) \cdot e^{i \cdot \varphi_\psi}$$

$$\boldsymbol{F_x = \frac{3}{2} \cdot \chi_{pm,R} \cdot i_d} \qquad \boldsymbol{F_y = \frac{3}{2} \cdot \chi_{pm,R} \cdot i_q}$$

Generic Complex Space Vector Modeling (3)

Linear-Rotary Machine

▼ Stator: 18 concentrated coils

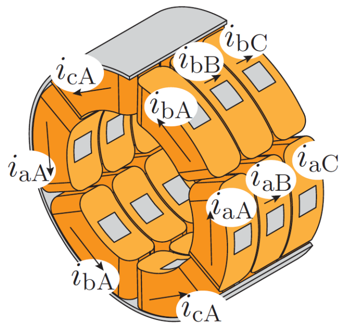

▼ PM Rotor: $N_{\mathrm{pp},R} = 4$

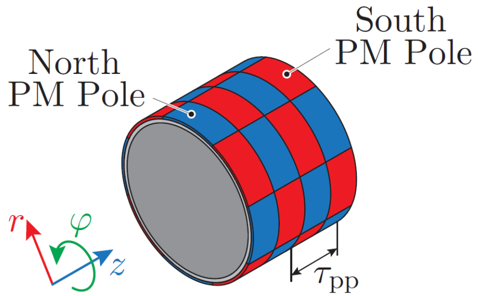

▼ Phase quantity

$$x_{\mathrm{aA}} = \hat{X}_{\mathrm{RL}} \cdot \cos(\omega_{\mathrm{R}} t + \varphi_x) \cdot \cos(\omega_{\mathrm{L}} t + \theta_x) \qquad \hat{X}_{\mathrm{RL}} \in \{\hat{U}_{\mathrm{RL}}, \hat{I}_{\mathrm{RL}}, \hat{\Psi}_{\mathrm{RL}}\}$$

▼ Double space vector transformation

$$\underline{\underline{x}} \triangleq \frac{4}{9} \begin{bmatrix} 1 & \underline{a} & \underline{a}^2 \end{bmatrix} \begin{bmatrix} x_{\mathrm{aA}} & x_{\mathrm{aB}} & x_{\mathrm{aC}} \\ x_{\mathrm{bA}} & x_{\mathrm{bB}} & x_{\mathrm{bC}} \\ x_{\mathrm{cA}} & x_{\mathrm{cB}} & x_{\mathrm{cC}} \end{bmatrix} \begin{bmatrix} 1 \\ \underline{b} \\ \underline{b}^2 \end{bmatrix} \qquad \underline{\underline{x}} \in \{\underline{\underline{u}}, \underline{\underline{i}}, \underline{\underline{\psi}}\}$$

$$\underline{a} = e^{\boldsymbol{i}(2\pi/3)} \qquad \underline{b} = e^{\boldsymbol{j}(2\pi/3)}$$

▲ Rotary $\boldsymbol{i}$ complex plane ▲ Linear $\boldsymbol{j}$ complex plane

Double Complex Space Vector

$$\underline{\underline{x}} = \underbrace{\hat{X}_{\mathrm{RL}} \cdot e^{i\cdot\varphi_x} \cdot e^{j\cdot\theta_x}} \cdot e^{i\cdot\omega_{\mathrm{R}} t} \cdot e^{i\cdot\omega_{\mathrm{L}} t}$$

$$\underline{\underline{x}}_{\mathrm{dq}} = \hat{X}_{\mathrm{RL}} \cdot e^{i\cdot\varphi_x} \cdot e^{j\cdot\theta_x} = x_{\mathrm{dd}} + i \cdot x_{\mathrm{qd}} + j \cdot x_{\mathrm{dq}} + i \cdot j \cdot x_{\mathrm{qq}}$$

▼ Flux linkage ($\varphi_\psi = 0$ and $\theta_\psi = 0$)

$$\underline{\underline{\psi}}_{\mathrm{dq}} = \psi_{\mathrm{dd}} = \hat{\Psi}_{\mathrm{RL}}$$

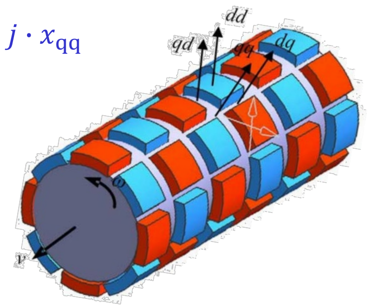

Source: Jin et al., 2012

Torque and Linear Force

$$\boldsymbol{T}_{\mathbf{z}} = \frac{9}{4} \boldsymbol{N}_{\mathbf{pp,R}} \cdot \hat{\boldsymbol{\Psi}}_{\mathbf{RL}} \cdot \boldsymbol{i}_{\mathbf{qd}} \qquad \boldsymbol{F}_{\mathbf{z}} = \frac{9\pi}{2\tau_{\mathbf{pp}}} \cdot \hat{\boldsymbol{\Psi}}_{\mathbf{RL}} \cdot \boldsymbol{i}_{\mathbf{dq}}$$

Bearing Force

- Rotary phase rescheduling needed

$$\boldsymbol{F}_{\mathbf{x}} = \frac{9}{4} \cdot \boldsymbol{\chi}_{\mathbf{pm,RL}} \cdot \boldsymbol{i}_{\mathbf{dd}} \qquad \boldsymbol{F}_{\mathbf{y}} = \frac{9}{4} \cdot \boldsymbol{\chi}_{\mathbf{pm,RL}} \cdot \boldsymbol{i}_{\mathbf{qd}}$$

Generic Complex Space Vector Modeling (4)

■ Linear Force Generation

- Simpler than full linear-rotary machine

▼ Stator: 9 concentrated coils

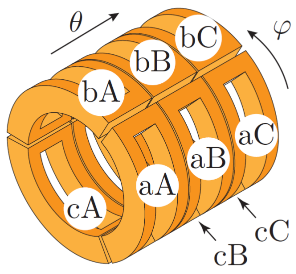

▼ PM Mover

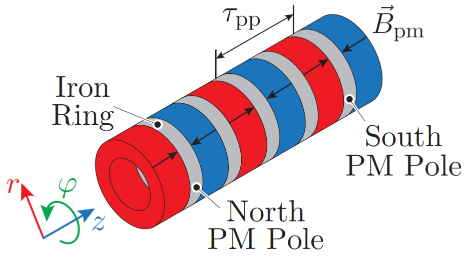

$$\underline{\psi}_{\mathrm{dq}} = \widehat{\Psi}_{\mathrm{M}}$$

$$\boldsymbol{F}_{\mathrm{z}} = \frac{9\pi}{\tau_{\mathrm{pp}}} \cdot \widehat{\Psi}_{\mathrm{M}} \cdot i_{\mathrm{q}}$$

■ Bearing Force Generation

- Linear-rotary machine with $\omega_{\mathrm{R}} = 0$

▼ Flux linkage

$$\underline{\underline{\psi}} = \underbrace{\chi_{\mathrm{pm,M}} \cdot (x + i \cdot y) \cdot e^{i\cdot\varphi_\psi} \cdot e^{j\cdot\theta_\psi}}_{} \cdot e^{j\cdot\omega_{\mathrm{L}}}$$

$$\chi_{\mathrm{pm,M}} = \frac{\mathrm{d}\widehat{\Psi}_{\mathrm{M}}}{\mathrm{d}x} = \frac{\mathrm{d}\widehat{\Psi}_{\mathrm{M}}}{\mathrm{d}y}$$

$$\underline{\underline{\psi}}_{\mathrm{dq}} = \chi_{\mathrm{pm,M}} \cdot (x + i \cdot y) \cdot e^{i\cdot\varphi_\psi} \cdot e^{j\cdot\theta_\psi}$$

$$\boldsymbol{F}_{\mathrm{x}} = \frac{9}{4} \cdot \chi_{\mathrm{pm,M}} \cdot i_{\mathrm{dd}}$$

$$\boldsymbol{F}_{\mathrm{y}} = \frac{9}{4} \cdot \chi_{\mathrm{pm,M}} \cdot i_{\mathrm{qd}}$$

Double Stator LiRA

Stator Arrangement
Cooling of Inner Stator
Geometry Optimization

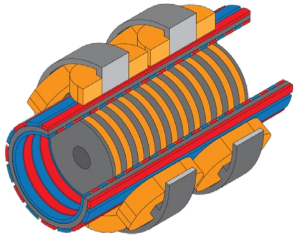

Double Stator (DS) LiRA Realization Options

- **Stator Arrangement**
  - Outer → Linear, Inner → Rotary

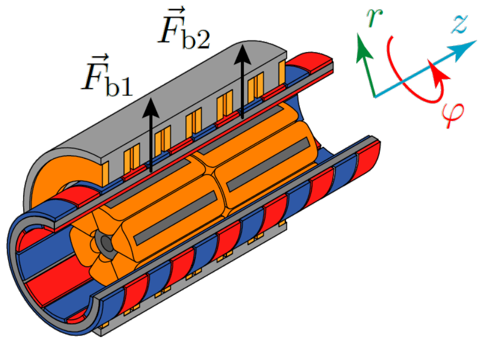

  - Outer → Rotary, Inner → Linear

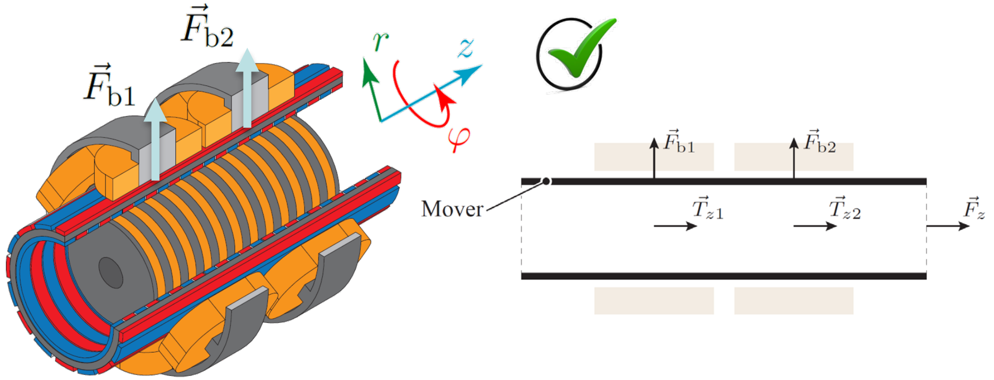

- **Mover Types**
  - With and Without Back Iron

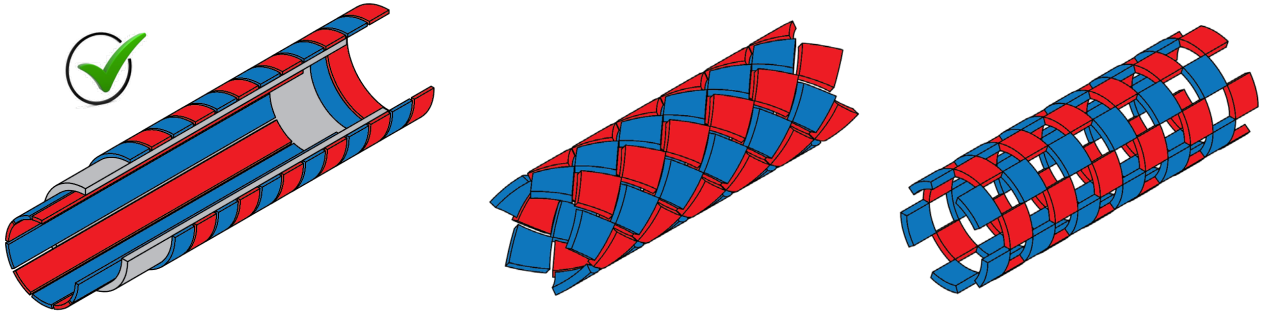

▲ CM ▲ DM ▲ SM

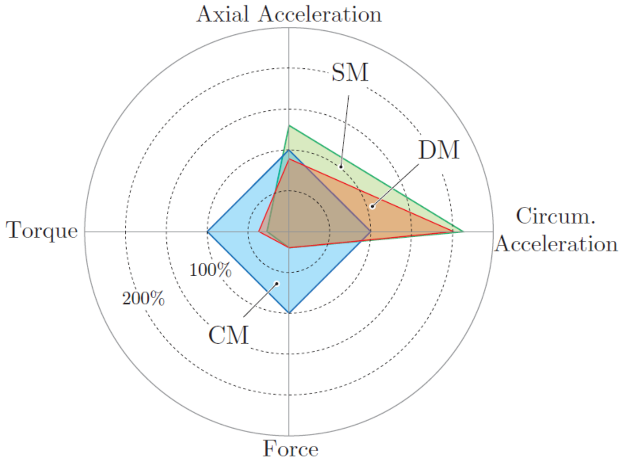

Cooling of the Inner Stator

Heat Flow Conduction Paths

- Outer Stator: Radial Heat Flow
- Inner Stator: Axial Heat Flow

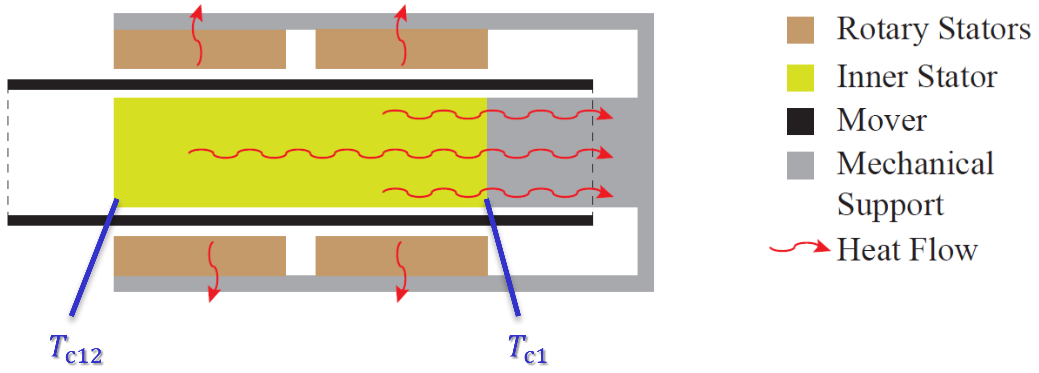

- Winding Temperature: $T_{c12} > T_{c1}$
- Unequal Temperature Distribution due to Axial Heat Flow and Thermal Resistance

Reduction of Axial Thermal Conductivity

- Iron Core Thermal Conductivity: $\sim 20\ \mathrm{W/(mK)}$
- Copper Pipe Thermal Conductivity: $\sim 400\ \mathrm{W/(mK)}$

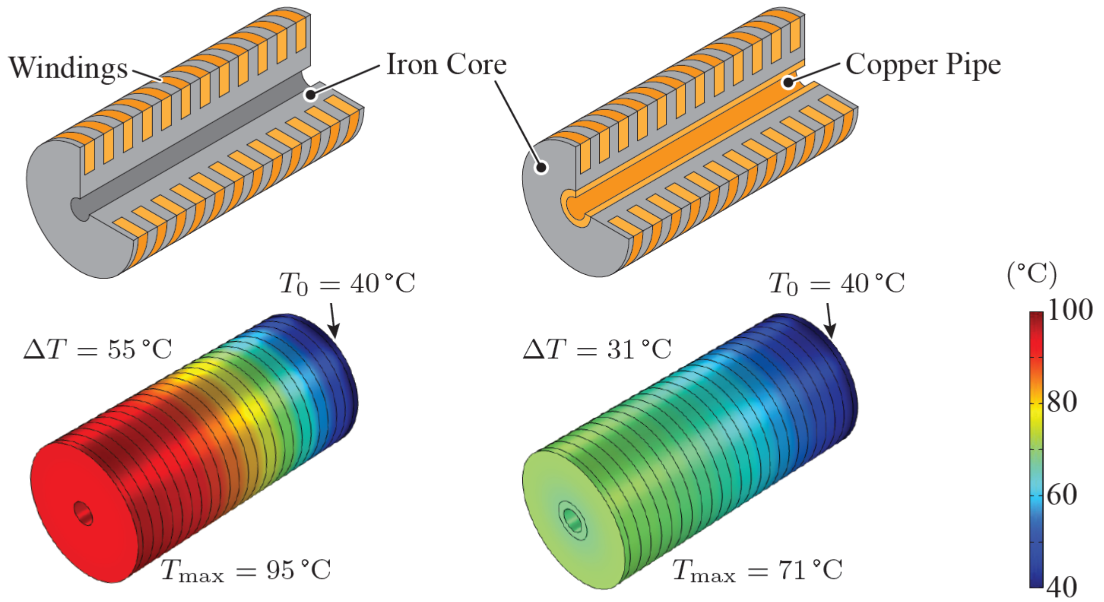

- Optimization Between ‘Magnetic’ and ‘Thermal’ Material

Analytic Thermal Model

- **Inner Linear Stator**
  - **Hot Spot Temperature: $T_{c12} < 120℃$**

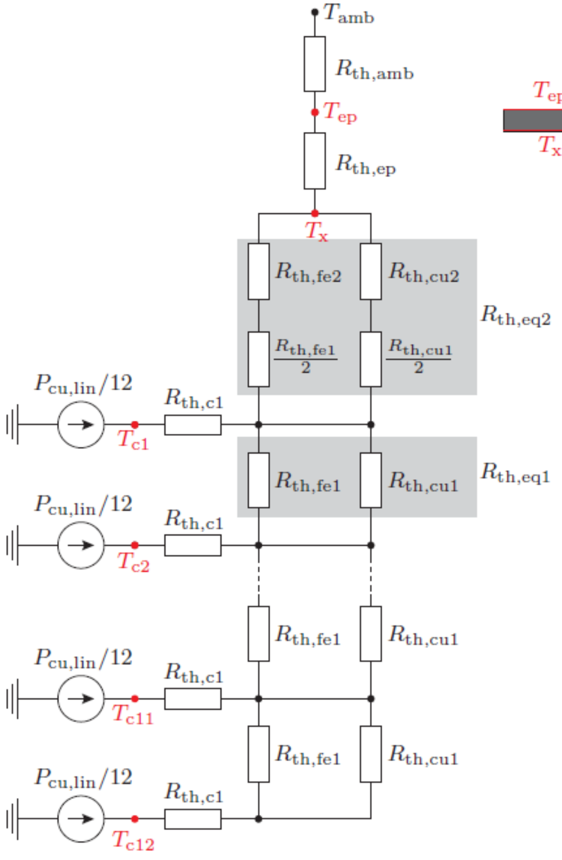

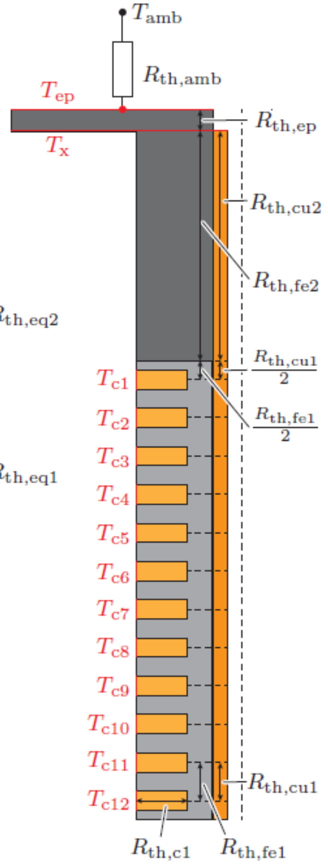

- **Outer Rotary Stators**
  - **Hot Spot Temperature: $T_{w1-6} < 120℃$**

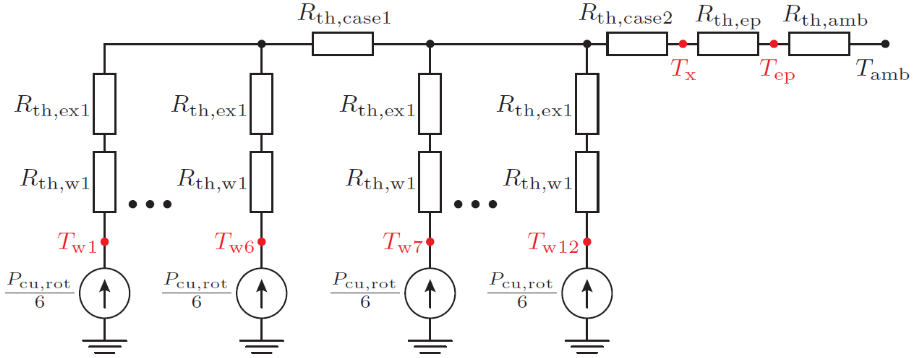

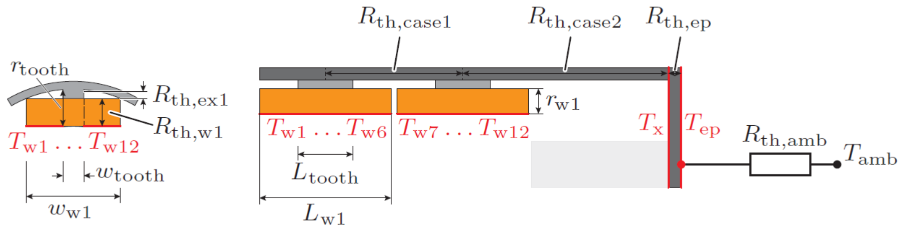

- **Thermal Model Equivalent Circuit**

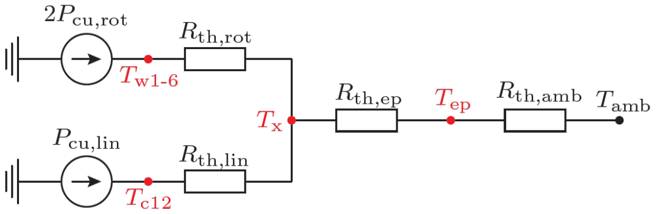

DS LiRA Geometry Optimization

- **Parametrize Geometry**
  - Outer Dimensions Fixed: $L = 100\ \mathrm{mm}, D = 100\ \mathrm{mm}$
  - Air Gaps: $r_{ag} = 0.7\ \mathrm{mm}$
  - Copper Pipe Hole: $D_{hole} = 8\ \mathrm{mm}$ (Sensor Cables)
  - Max. Winding Temp.: $120℃$

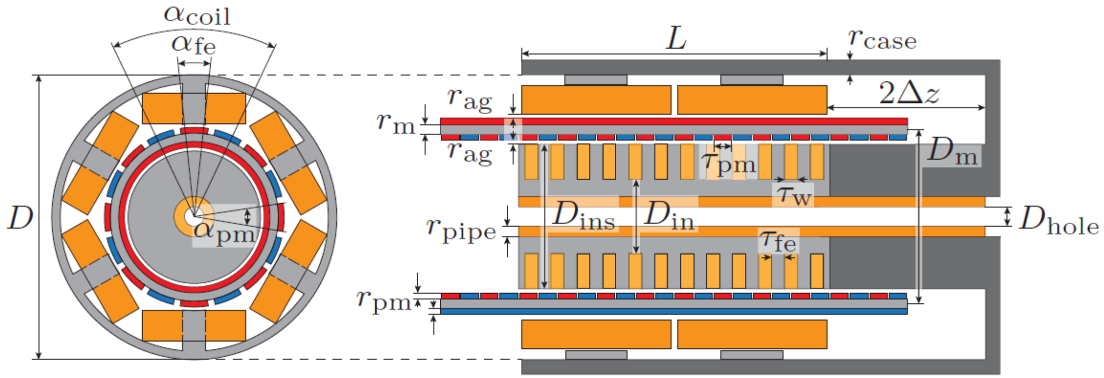

- **Models:**
  -Magnetic: 2D-FEM
  -Thermal: Analytic Lumped Parameter Circuit Network →

- **Automatized Optimization Procedure**
  - Discrete Design Space

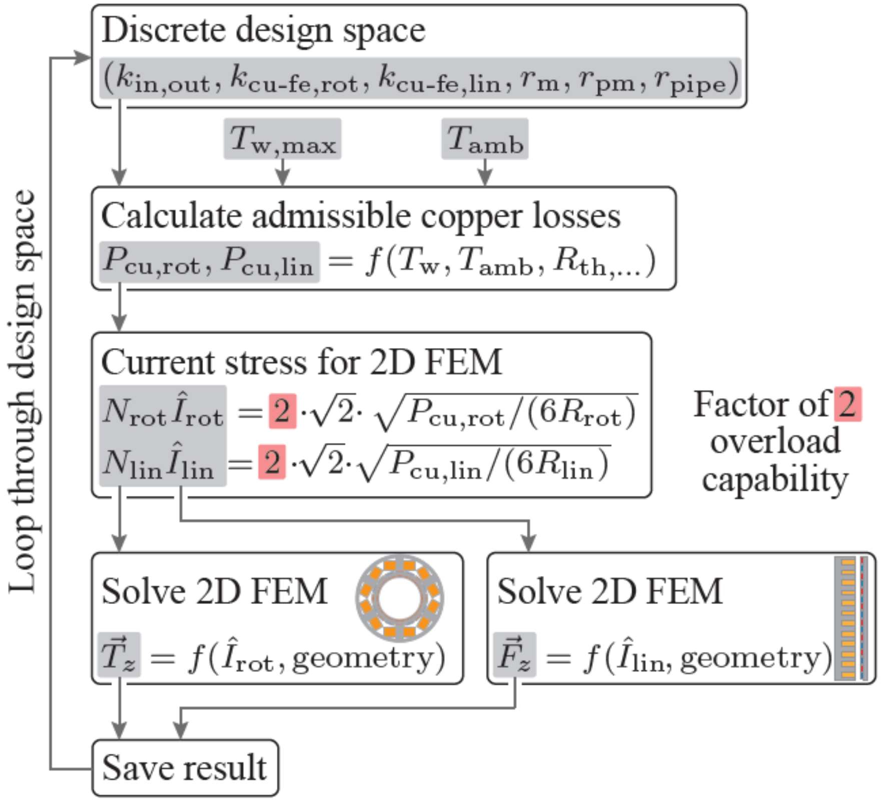

Optimization Results

- **Torque vs. Linear Force Pareto Plots**
  - **Compromise Between Torque/Force and Acceleration**

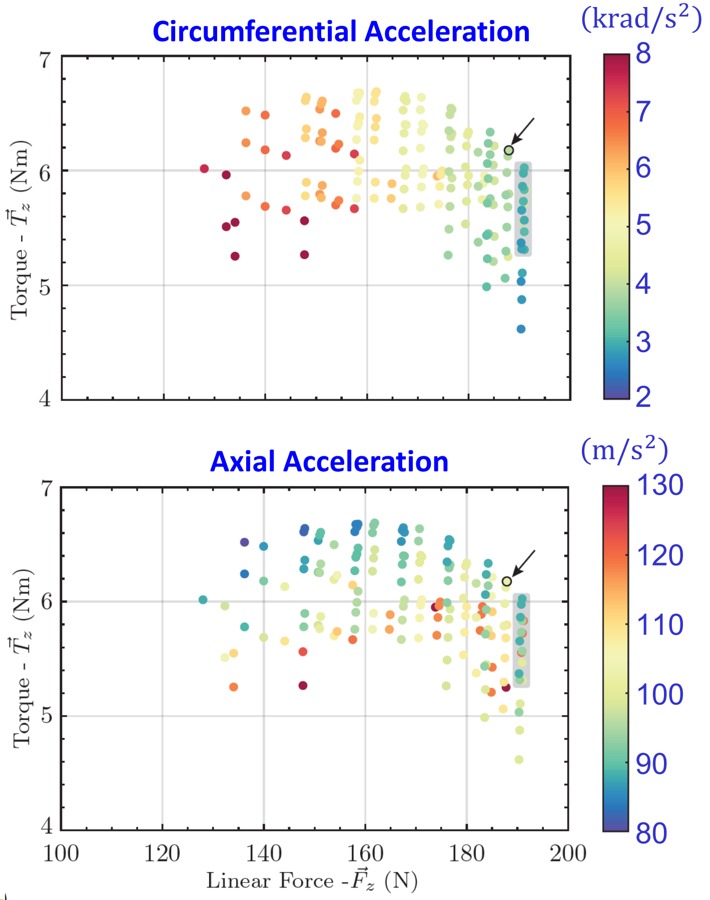

Chosen Design:
$5.3\ \mathrm{krad}/s^2$
$123.5\ \mathrm{m}/s^2$
$6.24\ \mathrm{Nm}$
$181.5\ \mathrm{N}$

- **3D FEM Flux Density Distribution in the Chosen Design**
  - **Flux Density Evaluated for Double the Continues Current**
  - **Outer stator: $< 2.1\ \mathrm{T}$, Inner Stator: $< 1.4\ \mathrm{T}$, Mover: $< 2.1\ \mathrm{T}$**

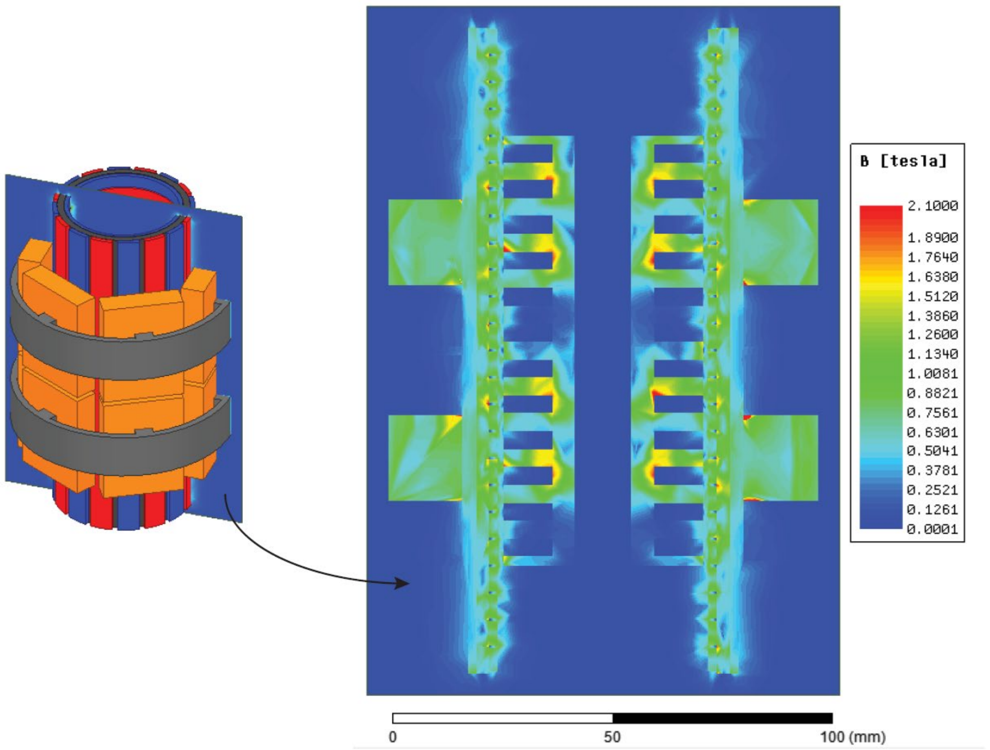

- **Hardware Prototype →**

DS LiRA Prototype

■ 3D CAD Model

- ‘Exploded View’ of the Outer Rotary and Inner Linear Stator

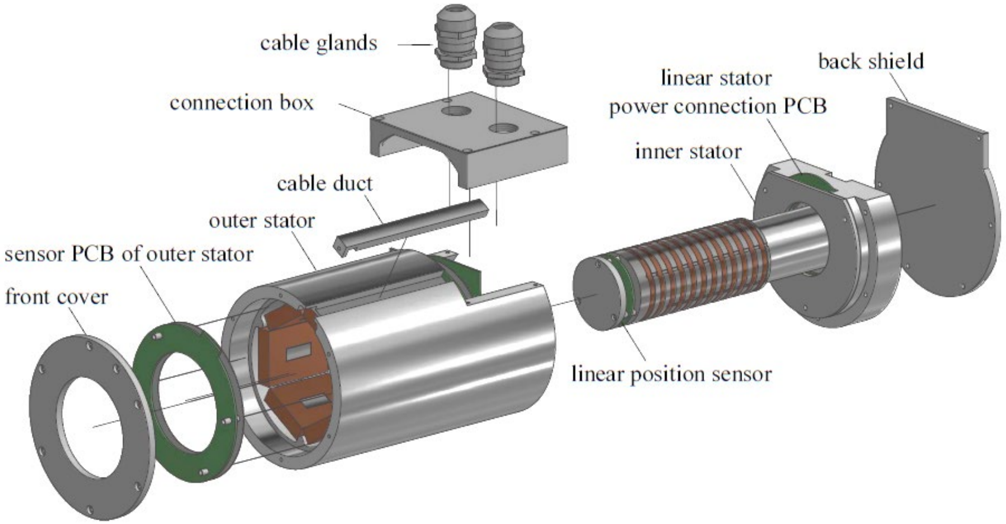

- Inner Stator: 12 × Coil Windings,
  1 × Lin. Pos. Sensor PCB,
  1 × Power Connection PCB
- Outer Stator: 12 × Concentrated Windings,
  2 × Rotary/Radial Pos. Sensor PCBs,
  1 × Power Connection PCB

■ Prototype Realization

- Outer Rotary Stator

- Inner Stator

- DS LiRA

- Mover

18-Phase Inverter Supply

Schematic

- *LC* Output Filter with Parallel *RC* Damping

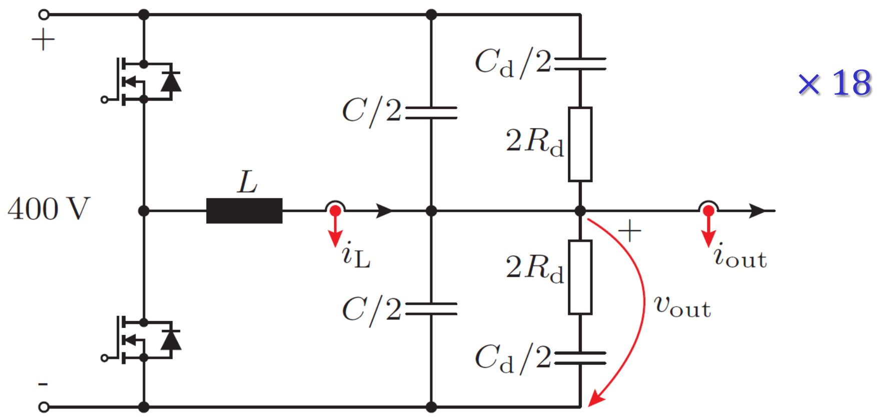

- Power Semiconductors: $600\ \mathrm{V}, 70\ \mathrm{m\Omega}, \mathrm{CoolGaN} - \mathrm{MOSFET}$
- Inductor: $L = 80\mu\mathrm{H}, \mathrm{N87}, \mathrm{RM12}, 23\ \mathrm{Turns}, 71\mu\mathrm{m\ Strand}$
- Capacitance: $C = 4.8\mu\mathrm{F}$ for $THD_{vout} = 1\%$
- Heatsink Design: $CSPI = 12\ \mathrm{W}/(\mathrm{K}dm^3)$

Hardware Realization

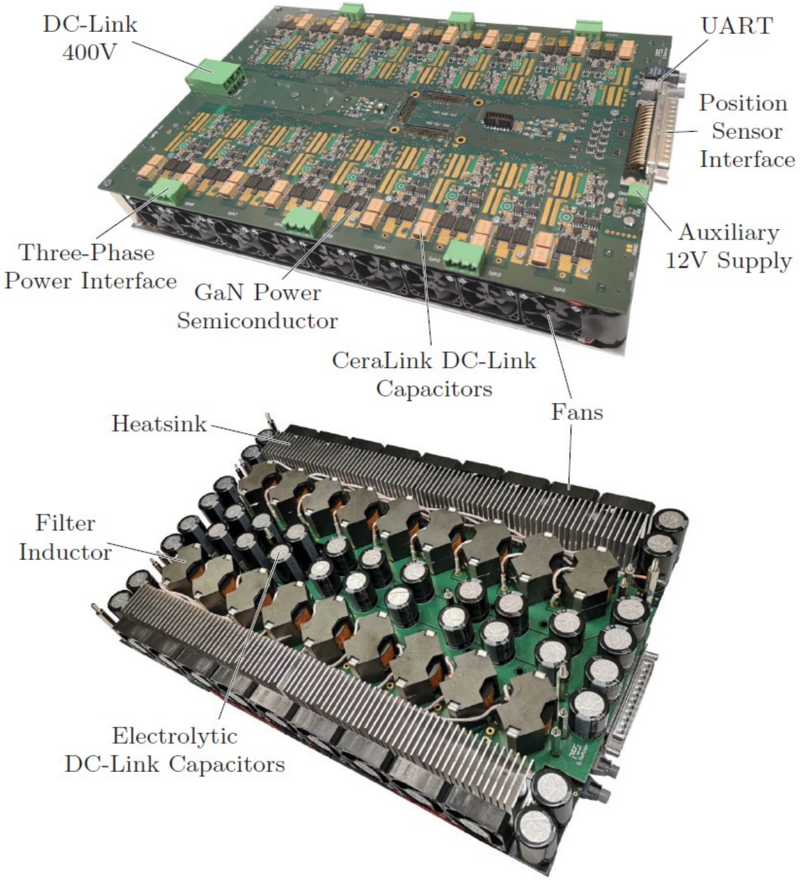

Current & Position Controller

- **Current Control Structure**
  - **Input: i_{out} References → From the Position Controller**

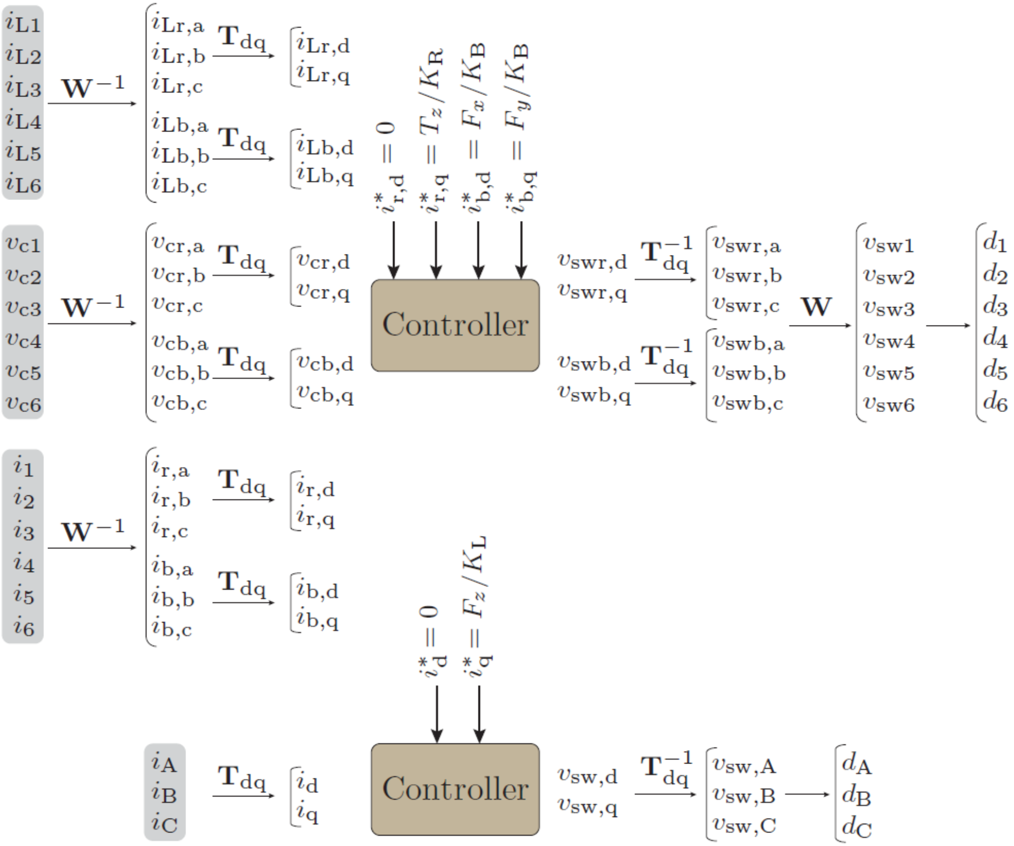

- **'Decentralized' Position Control**
  - **Dedicated PID Controller for Each Motion Mode**

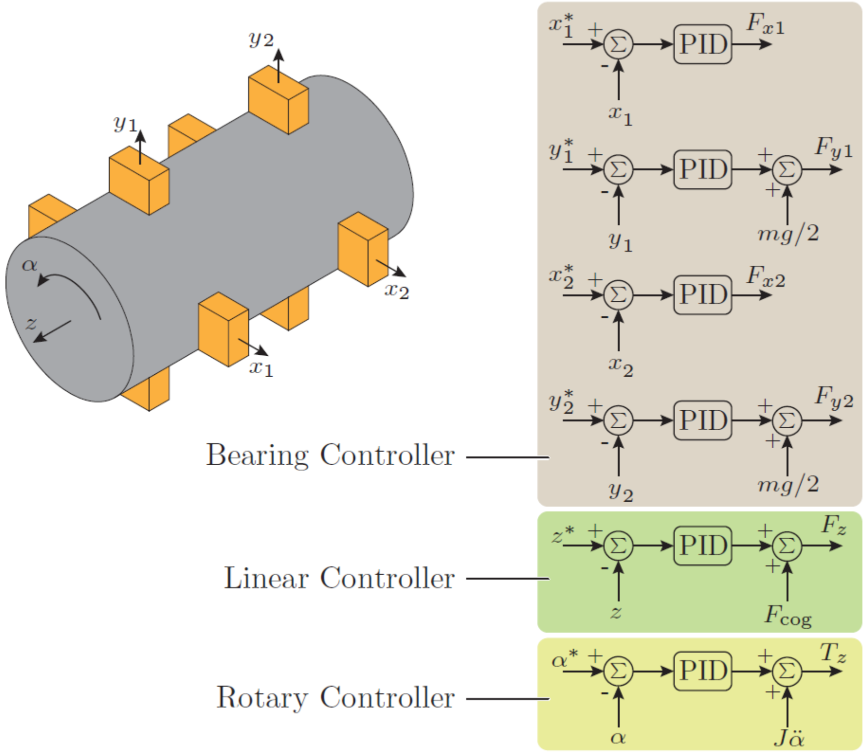

DS LiRA Measurement Results

Rotary Step

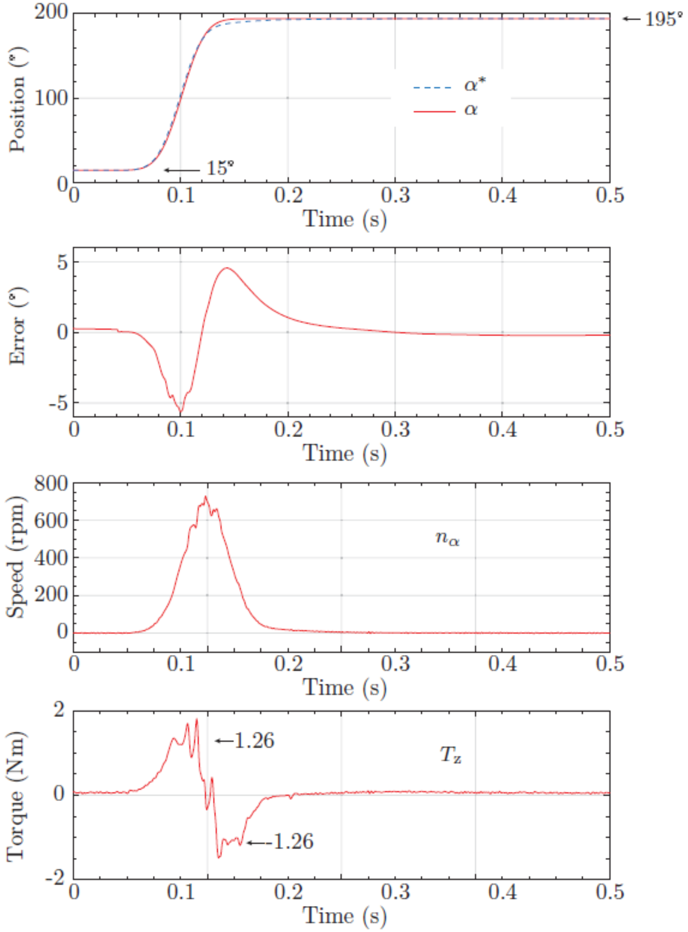

Stroke: **180 °**

Error: < |±5| °

Max. Speed: **~700 rpm**

Torque Limit: **±1.26 Nm**

Rotary Step: Radial Positions

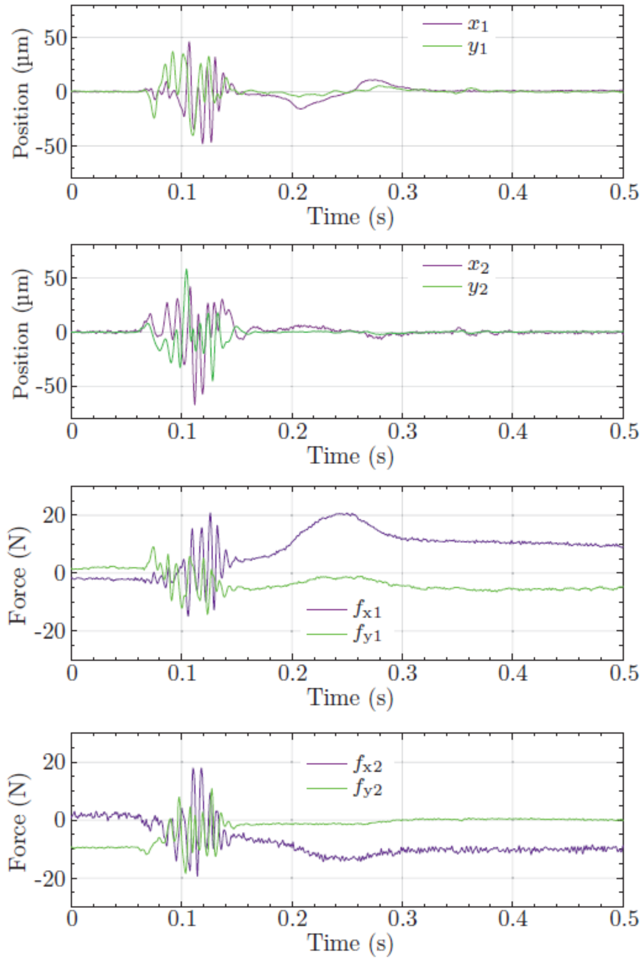

References:
$x_1^* = 0$
$y_1^* = 0$
$x_2^* = 0$
$y_2^* = 0$

Deviations: **±50 µm**

DS LiRA Measurement Results

- Video

Summary

- **Linear Bearingless Actuator**

  - Integration of Magnetic Bearings into a Linear Actuator
  - Radial Position and Tilting Control in Micro Meter Range
  - High-Precision/Purity/Dynamic Linear Motor Applications

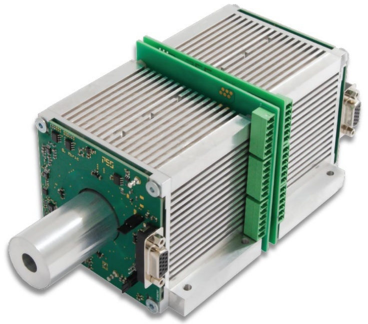

- **Linear-Rotary Bearingless Actuator**

  - Coupling of Rotation, Linear Motion, Magnetic Bearings
  - Automatized Semi-Numerical Optimization Procedure
  - High-Precision/Purity Applications

Biography of the Speaker

Spasoje Miric received B.Sc., M.Sc., and Ph.D. degrees in electrical engineering from the University of Belgrade, School of Electrical Engineering in 2012, 2013, and 2018, respectively, focusing on power electronics systems and drives. In 2021 he defended his second Ph.D. thesis at ETH Zurich at the Power Electronic Systems Laboratory (PES) in the advanced mechatronic systems area. More specifically, during his Ph.D. project, he focused on linear-rotary actuator systems with magnetic bearings, resulting in two new machine topologies patented. Since 2021, he has been with PES as a post-doc researcher, focusing on WBG power converter optimization with hard and soft-switching, new modulation techniques of flying capacitor converters, wireless power transfer systems, and eddy-current-based position sensor systems.

He was appointed Ass. Professor and Head of the Innsbruck Drives and Energy Systems Laboratory at the University of Innsbruck (UIBK) on Jan. 1, 2023. DDr. Miric proposed a novel self-bearing actuator topology and a generalized complex space vector calculus for linear-rotary machines. He has published 20+ scientific papers in international journals and conference proceedings and filled 7 patents. He has presented 2 educational seminars at leading international conferences and received 5 IEEE Transactions and Conference Prize Paper Awards.

Since 01.01.2023:

Drive and Energy Systems Laboratory (i-DES)

www.uibk.ac.at/mechatronik/ides/

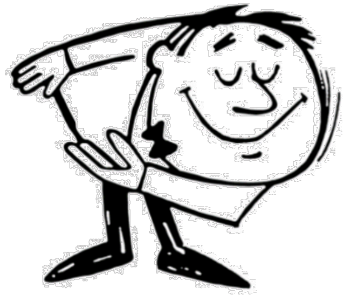

Thank you!